Int J Adv Manuf Technol (2016) 87:2221–2244
DOI 10.1007/s00170-016-8567-7

ORIGINAL ARTICLE

Performance comparison of wiper and conventional ceramic inserts in hard turning of AISI 4140 steel: analysis of machining forces and flank wear

H. Aouici [1,2] · M. Elbah [1,2] · M. A. Yallese [1] · B. Fnides [1,3] · I. Meddour [1,2] · S. Benlahmidi [2]

Received: 16 November 2015 / Accepted: 29 February 2016 / Published online: 23 March 2016

Abstract This paper describes a comparison of machining forces and flank wear between wiper ceramic (multi radii) and conventional ceramic cutting tools in dry hard turning of cold work tool steel AISI 4140 (60 Hardness Rockwell Cone (HRC)) using the Response Surface Methodology (RSM). For this purpose, a number of machining experiments based on statistical three-factor (cutting speed, feed rate, and depth of cut) and three-level factorial experiment designs completed with a statistical analysis of variance (ANOVA) were performed. From the parametric analysis, it is revealed that the uncoated ceramics (CC650WG wiper and CC650 conventional) performs better than the coated ceramics (CC6050WH wiper and CC650 conventional) with reference to machining forces. On the contrary, wiper ceramic cutting tools (CC6050WH and CC650WG) have the better performance compared with conventional ceramic cutting tools (CC6050 and CC650), in particular, the flank wear.

Keywords Hard turning · AISI 4140 steel · Ceramic · Wiper · ANOVA · RSM

✉ H. Aouici
aouici_hamdi@yahoo.fr

[1] Laboratoire Mécanique et Structures (LMS), Département de Génie Mécanique, FST, Université 08 Mai 1945, 24000 Guelma, Algeria

[2] Ecole Nationale Supérieure de Technologie, Algiers, Algeria

[3] Département de Construction Mécanique et Productique, FGM&GP, USTHB, BP 32 El-Alia, Bab-Ezzouar, 16111 Algiers, Algeria

1 Introduction

The term "ceramics" is applied to a range of inorganic materials of widely varying uses. Generally, these materials are non-metallic, and in most cases, have been treated at a high-temperature at some stage during manufacture. Ceramics are far less ductile than metals and tend to fracture immediately when any attempt is made to deform them by mechanical work [1, 2]. They are often of complex chemical composition and their structures may also be relatively complex. Ceramic tools have high resistance to heat and wear and can therefore be used to machine metals that are extremely hard; they are also chemically stable. These attributes allow them to be used to machine metals at high cutting speeds and in dry machining conditions because it is not necessary to reduce the temperature on the cutting edges of these tools. However, in machining, these favorable properties are exchanged for reduced toughness when these tools are compared with carbide tools. This deficiency can be offset by selecting an appropriate ceramic cutting grade and type of tool. Ceramic tools are based primarily on alumina (Al_2O_3) and silicon nitride (Si_3N_4) compounds and are available in a variety of grades that include ceramics mixed with other materials and reinforcing whisker materials that make them harder [3, 4].

A comprehensive review shows several studies related to cutting forces and flank wear in finish turning process with ceramic cutting tools. Recently, Fnides et al. [5] performed turning of hardened steel AISI 4140 using mixed ceramic and reinforced ceramic tools, respectively. The results concluded that the machining with the mixed ceramic insert generates lower values of cutting force components than reinforced ceramic insert. In another study, Aouici et al. [6] studied the effects of cutting speed, feed rate, and depth of cut on cutting force, specific cutting force, and power in machining AISI D3 cold work steel with TiN-coated mixed ceramic

insert CC6050 in the turning operation. They analyzed the process constraints on performance characteristics using analysis of variance (ANOVA). They concluded that feed rate and depth of cut strongly control the cutting force, specific cutting force, and power. Besides, Hessainia et al. [7] experimentally investigated the influences of machining conditions, including cutting parameters (Vc, *f*, and ap) and cutting tool vibrations on surface roughness criteria in hard machining of 42CrMo4 steel (56 Hardness Rockwell Cone (HRC)) using Al_2O_3+ TiC mixed ceramic tool and established a correlation between tool vibrations and surface roughness by approaching Response Surface Methodology (RSM). Their experimental results stated that feed rate is the prominent parameter in determining the surface roughness, while tool vibrations have less influence on surface roughness. Moreover, Fnides et al. [8] have established statistical models of the cutting forces in hard turning of AISIH11 hot work tool steel and analyzed the effect of the main cutting variables, such as cutting speed, feed, and depth of cut on cutting force components using Al_2O_3+ TiC mixed ceramic tool. Luo et al. [9] have investigated the relationship between hardness and cutting forces during turning AISI4340 steel hardened from 29 to 57 HRC using mixed alumina tools. The results suggest that an increase of 48 % in hardness leads to an increase in cutting forces from 30 to 80 %. In finish hard machining with coated ceramics, Lalwani et al. [10] applied chamfered and honed edges to identify the effect of cutting parameters on cutting forces and surface roughness. They found that cutting speed has no significant effect on cutting forces and surface roughness in the range of 55–93 m/min. Also, the thrust and cutting forces were significantly affected by both the feed rate and depth of cut. Besides, Kumar et al. [11] found that flank wear increased with increasing cutting speed in both types of ceramic cutting tools. The flank wear, crater wear in Ti (C, N) mixed alumina ceramic tool was lower than that of SiCW reinforced alumina cutting tool on machining martensitic stainless steel-grade 410 (60 HRC) and EN24 steel (45 HRC).

To improve the performance of the cutting tools, developments in tool geometry were done. For instance, multi radii (wiper) technology has been analyzed in hard turning. This technology is based on the use of multi radii tool nose. Thus, the use of multi radii tools provides a higher contact area than the one generated by conventional tools [12]. The use of multi radii tools provides excellent surface roughness values, even at high feed rates. The surface roughness obtained using conventional and multi radii tools was compared by Grzesik [13], who performed an extensive study characterizing the surface roughness generated during hard turning with conventional and wiper ceramic tools at a variable feed rate. A similar study was also reported by Grzesik and Wanat [14]. In the same way, a comparative study among these tools was also carried out by Davim et al. [15]; it was revealed that, the wiper ceramic insert performed better with reference to surface roughness and tool wear, while the conventional insert was useful in reducing the machining force and power. The experimental studies by Elbah et al. [16] applied response surface methodology and ANOVA to investigate the machinability of hardened AISI 4140 cold work tool steel using a range of cutting tools. The results indicated that surface roughness of AISI 4140 steel was improved as cutting speed was elevated and deteriorated with feed rate. However, the surface quality obtained with the wiper ceramic insert allowed a surface finish as good when compared with conventional ceramic insert is 2.5.

From the above-mentioned literature, the researchers mainly compared the machining forces of the turning process in hardened steel metals when using various cutting tools. The investigations executing the turning operations also found the machining forces of steel-alloys were created by the prediction models (using DOE). The aim of the study is to evaluate and compare the performance of the fourth ceramic cutting tools, namely, wiper and conventional ceramic tools (CC6050WH, CC6050, CC650WG, and CC650) when in hard turning of AISI 4140 (60 HRC). The following aspects of the process are addressed: machining forces and flank wear.

2 Experimental procedure

Turning experiments were performed in dry conditions using a universal lathe type SN 40C with 6.6 kW spindle power, equipped with a commercial tool holder having the following geometry: rake angle $\gamma = -6$ ° (negative), clearance angle $\alpha = 6$ °, and side cutting edge angle $\chi = 75$ °. Type inserts ceramic tools reference CC6050WH (wiper coated with TiN), CNGA120408S01525WH; reference CC6050 (conventional coated with TiN), CNGA120408S01525; reference CC650WG (uncoated wiper), CNGA120408S01525WG; and reference CC650 (uncoated conventional), CNGA120408S01525 were used to machine the AISI 4140. All ceramic tools have the same chemical composition with Al_2O_3 (70 %) and TiC (30 %). The tool holder PCBNR2525M12 was used during hard turning. The wiper tool nose radius geometry is shown in Fig. 1.

The material used for this investigation was AISI 4140 hardened steel with a hardness of 60 HRC in the form of a round bar with an external diameter of 72 mm. This workpiece material was selected based on its applications in automotive, crank shafts, spindles, connecting rods, pump, gear shafts, tie rods, and bolts, requiring high resistance. Also, the AISI 4140 steel is used for making jigs and frames, support tools, forging dies, etc. [16]. The following chemical compositions (in wt%): C 0.43, Mn 0.79, Si 0.24, S 0.024, Cu 0.025, Al 0.029, Ti 0.004, Nb 0.001, Ni 0.022, Cr 1.10, Mo 0.19, Va 0.005, Sn 0.002, and Fe in balance.

The setup used to measure the three components of the cutting force (machining forces), axial force (Fa), radial force

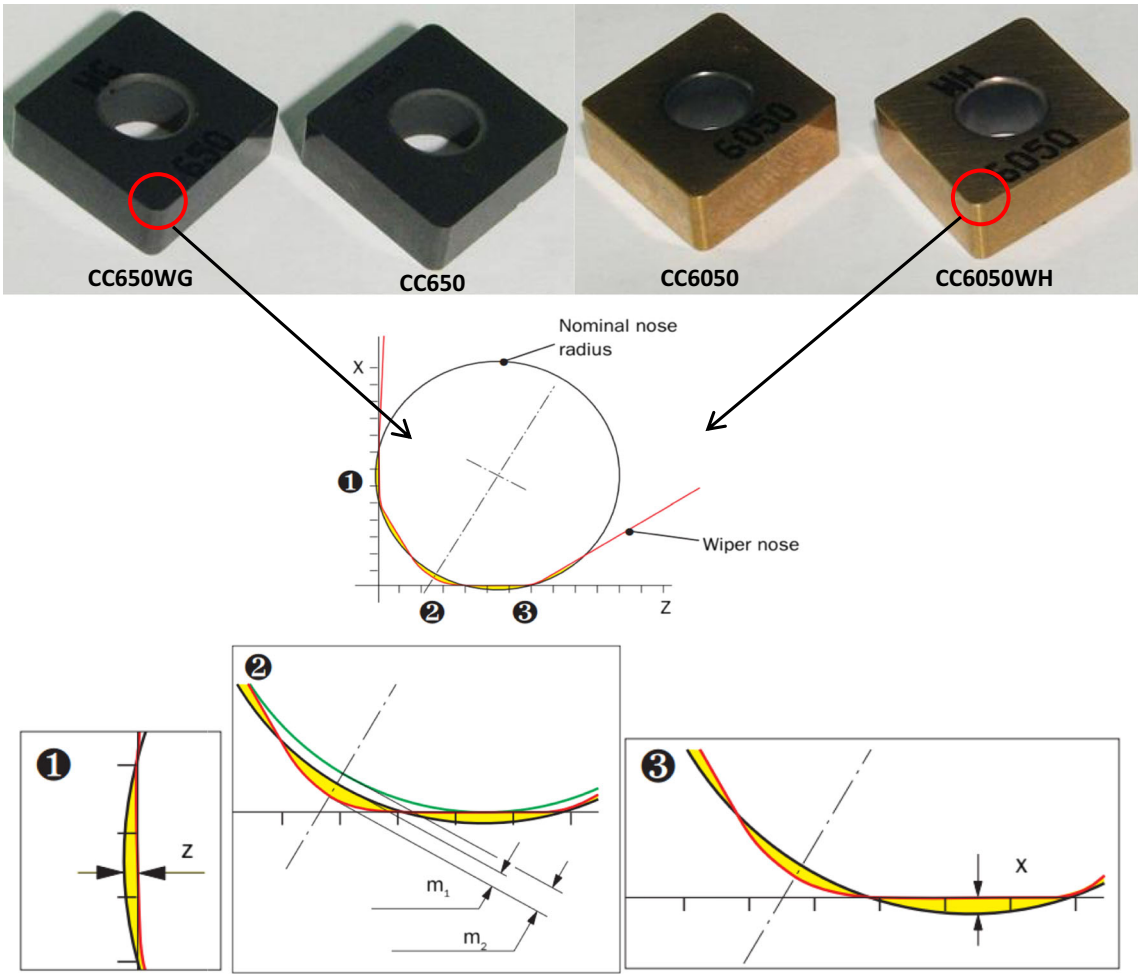

Fig. 1 Cutting inserts

(Fr), and tangential force (Ft). The tool holder is mounted on a four-component piezoelectric dynamometer (Kistler 9257B), schematically shown in Fig. 2. The measurement chain also included a charge amplifier, data acquisition hardware (A = D2855A3), and graphical programming environment (DynoWare 2825A1-1) for data analysis and visualization. The flank tool wear was evaluated by a "Visual machine 250 tool makers" microscope with ×4.5 magnification and 1-μm resolution. The admissible wear was established according to ISO 3685 standard (1993).

3 Results and discussion

3.1 Parametric influence on machining forces

The machining forces (cutting force components) acting on tool is an important aspect in hard machining. The machining forces directly influence on heat generation, tool wear, quality of machined surface, and accuracy. Thus, in the present work, influence of cutting parameters on machining forces during machining of AISI 4140 steel hardened to 60 HRC with four ceramic cutting tools, namely, wiper and conventional ceramics have been compared.

The results in Fig. 3 illustrate the evolution of machining forces depending on the cutting speed for the following ceramics: CC6050WH, CC6050, CC650WG, and CC650 at constant feed rate of 0.08 mm/rev and depth of cut of 0.20 mm. Analysis of the results shows that increasing the cutting speed generally leads to a reduction of machining forces (Fa, Fr, and Ft). This trend is mainly due to increase in temperature at shear plane region, resulting in the plastic softening of this primary deformation zone and hence reduced shear strength of the material. This will, in turn, reduce the force required to deform the material to be machined [17]. Regarding the curve trends, the machining forces decreased as Vc increased to 160 m/min; beyond this value, they stabilized. The decrease in the machining forces is more expressed at low speeds. In fact, an increase of Vc from 45 to 160 m/min cause a drop of the three components (Fa, Fr, and Ft) at 45.01, 50.84, 55.46, and 36.55 % of the axial force; 69.77, 43.36, 66.36, and 43.77 % of the radial force; and (22.52, 37.92,

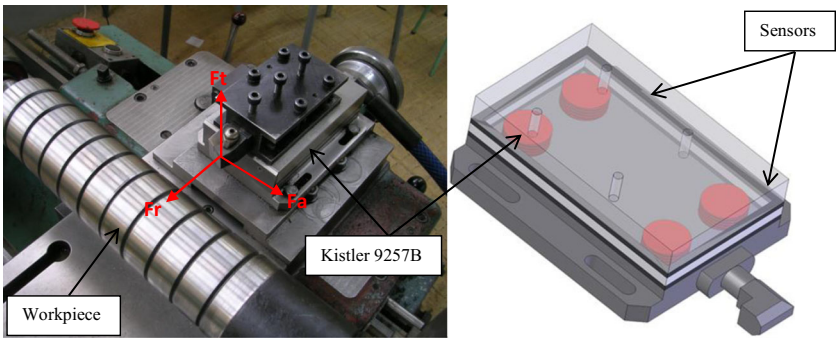

Fig. 2 Experimental configuration for measuring the components of cutting force

36.66, and 52 % of the tangential force to the different cutting ceramics (CC6050WH, CC6050, CC650WG, and CC650), respectively, while an increase of *Vc* from 160 to 350 m/min caused a drop ratio of 21.90, 33.10, and 48 %, respectively. The second zone from 160 to 350 m/min is characterized by an interval where the machining forces are stabilized. In practice, this zone constitutes the optimal range of use of the cutting edge. This minimizes the constraints which cause the requests and abrupt rupture of the cutting edge.

The curve of Fig. 4 illustrate the evolution of the machining forces according to the feed rate for the following ceramics: CC6050WH, CC6050, CC650WG, and CC650 at constant cutting speed of 160 m/min and depth of cut of 0.20 mm. It is noticed that with the increase in feed rate, the machining forces increase. The increased feed rate increases cutting forces. As the feed rate is increased, the region of sheared chip increases, since resistance to material rupture is higher and hence requires larger efforts for chip removal [18, 19]. Similar results were reported by Aouici [6] when turning AISI D3 steel (60 HRC) using CC6050 tool. It is noticed that the radial force is dominating compared to both others and that for all the feed rates and for all cutting tools tested. The effects of the feed rate on the machining forces are as follows: the increase in the feed rate from 0.08 to 0.28 mm/rev increases the components of the machining forces 37.56, 2.36, 74.17, and 26.79 % of the axial force to 103.53, 35.76, 131.30, and 48.07 % of the radial force and 92.38, 110.88, 145.67, and 175.85 % of the tangential force to different cutting ceramics (CC6050WH, CC6050, CC650WG, and CC650), respectively. It is noted that the tangential force is very affected by the feed rate, follow-up of the radial force, and lastly, of the axial force. As the feed rate is increased, the region of sheared chip increases, since resistance to material rupture is higher and hence requires larger efforts for chip removal [18]. Similar results were observed by Aouici et al. [20] when turning AISI H11 steel (50 HRC) using the CBN7020 tool.

The results obtained in Fig. 5 illustrate the evolution of machining forces according to the depth of cut at constant cutting speed of 160 m/min and feed rate of 0.08 mm/rev. The analysis of the effect of depth of cut on machining forces shows that this parameter has a very significant influence. This is because increased depth of cut results in increased tool work contact length [21]. Subsequently, chip thickness becomes significant that it causes the growth of the volume of

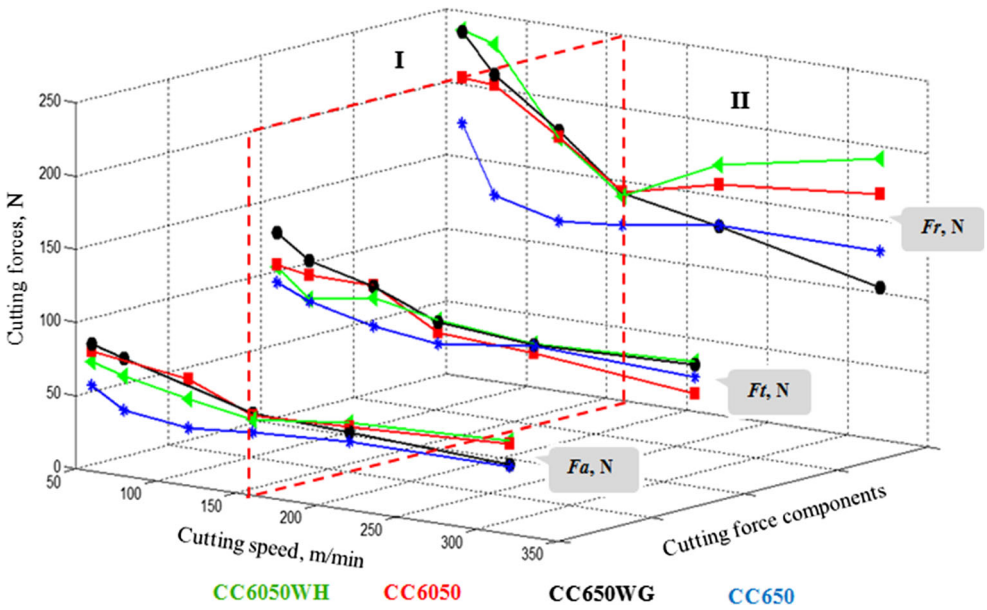

Fig. 3 Effect of cutting speed on machining forces at constant $f = 0.08$ mm/rev and ap = 0.20 mm (CC6050WH, CC6050, CC650WG, and CC650)

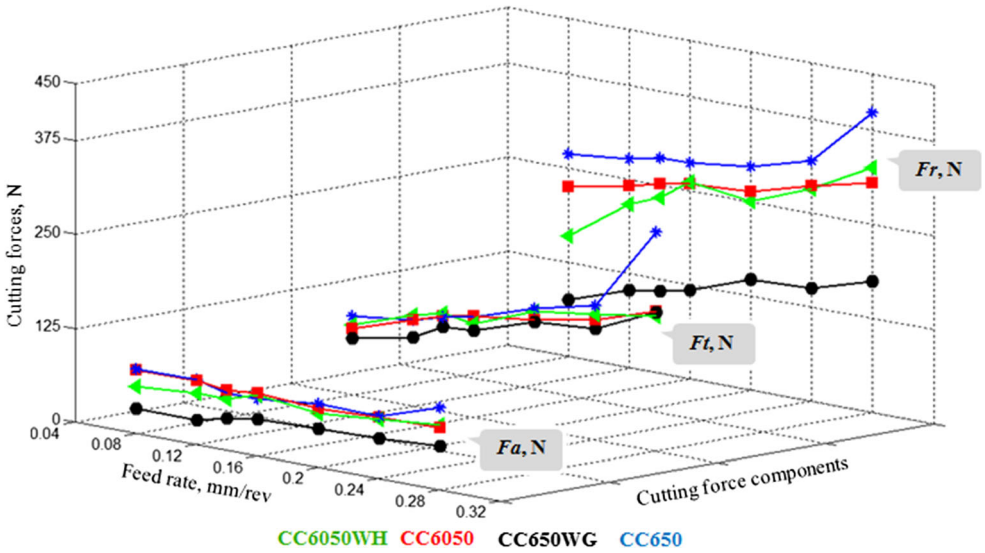

Fig. 4 Effect of feed rate on machining forces at constant ap = 0.20 mm and Vc = 150 m/min (CC6050WH, CC6050, CC650WG, and CC650)

deformed metal and requires greater cutting forces to cut the chip. On a practical level, the increase in the depth of cut from 0.10 to 0.70 mm increases the cutting force components (Fa, Fr, and Ft) from 628.96, 270.49, and 82.30 % for TiN-coated wiper ceramic CC6050WH and from 876.07, 116.23, and 356.24 % for TiN-coated conventional ceramic CC6050 and 828.19, 47.75, and 278 15 % for the uncoated wiper ceramic CC650WG and 644.09, 144.18, and 495.60 % for uncoated conventional ceramic CC650.

3.2 Flank wear

Tool wear is one of the most important criteria in machining processes; it directly affects the tool life, surface quality, and production cost. Tool wear in machining AISI 4140 material occurs due to the rubbing of the cutting tool edge with the work piece. While machining AISI 4140 steel, flank wear is the main form of wear, as other forms of tool wear are negligible for all cutting materials. The long duration tests of straight turning on AISI 4140 steel treated at 60 HRC are carried out. The purpose of these operations is to determine the wear curves as a function of cutting time and therefore the tool life of fourth cutting materials (CC6050WH, CC6050, CC650WG, and CC650).

Figure 6 shows the flank wear variation with cutting time at 150 m/min and feed rate at 0.08 mm/rev for the following ceramics: CC6050WH, CC6050, CC650WG, and CC650, respectively. Figure 6 clearly shows that the best results were attained when machining with CC6050WH and CC650WG tools, followed by CC6050 and CC650 tools, respectively. According to the curve of TiN-coated wiper ceramic inserts CC6050WH and for a machining time of 5 min, the flank wear

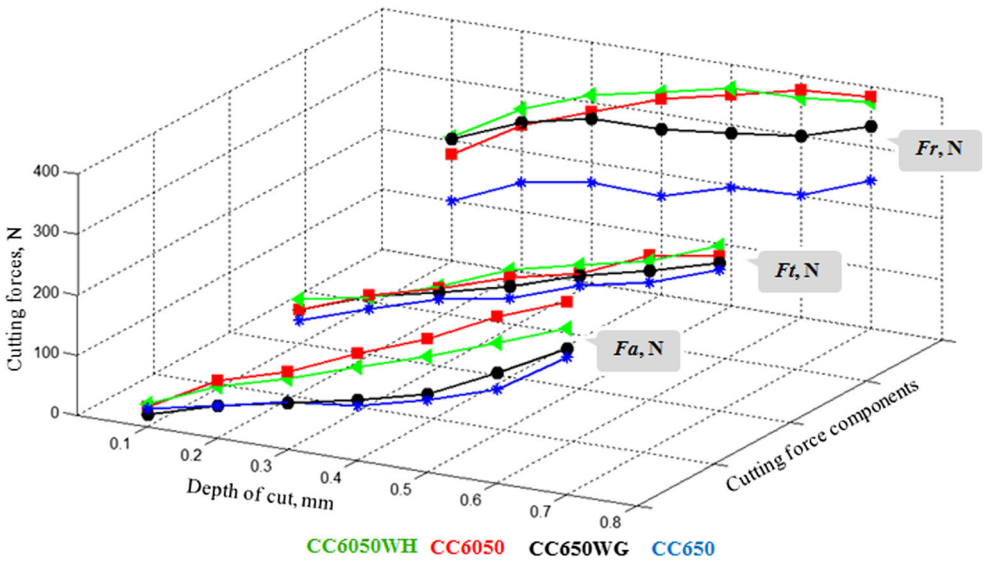

Fig. 5 Effect of depth of cut on machining forces at constant f = 0.08 mm/rev and Vc = 150 m/min (CC6050WH, CC6050, CC650WG, and CC650)

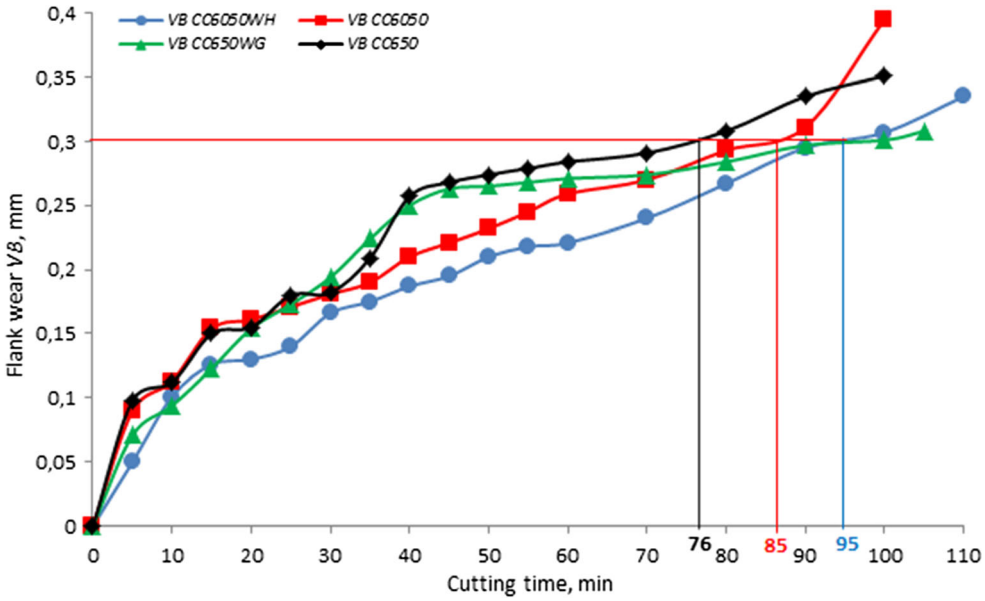

Fig. 6 Flank wear (VB) evolution as a function of cutting time at various cutting tools (CC6050WH, CC6050, CC650WG, and CC650)

VB of this insert reaches a value of 0.05 mm. At the end of machining $t = 95$ min, the flank wear is 0.30 mm. This change represents an increase of 500 %. The first machining test done with the uncoated ceramic inserts CC650WG generates a flank wear of 0.071 mm. For a machining time of 5 min, its wear VB is 0.30 mm, which defines the lifespan of this tool 95 min.

The micrographs of flank wear at Vc = 150 m/min, ap = 0.20 mm, and $f = 0.08$ mm/rev of CC6050WH, CC6050, CC650WG, and CC650 are presented in Fig. 7. We can see that the flank wear evolution is regular. In addition, Fig.7a–d show the micrographs of the worn mixed ceramic cutting tools. The main wear mechanism observed is abrasive wear, with deeper grooves when compared with the parallel marks on the flank face of the ceramic cutting tools. This could be a result of fragments of the carbide grains that are pulled out from the tool surface, dragged across the flank face, thus removing the tool material. Also, the cutting edge does not present chipping, demonstrating a good stability during the cutting process. The flank wear in this stage was 0.3 mm.

4 RSM experimental design

Response surface methodology is a collection of mathematical and statistical techniques that are useful for the modeling and analysis of problems in which a response of interest is influenced by several variables and the purpose is to optimize this response [22]. RSM comprises the following six major components: (1) defining the independent input variables and the desired output responses, (2) adopting an experimental design plan, (3) performing regression analysis with the quadratic regression models of RSM, (4) calculating the ANOVA for the independent input variables in order to find parameters which significantly affect the response, (5) determining the situation of quadratic regression models of RSM, and finally, (6) optimizing and conducting confirmation experiment and verifying the predicted performance characteristics.

In the current study, the relationship between the input, called the cutting conditions (cutting speed (Vc), feed rate (f), and depth of cut (ap) and the output Y define as a machinability aspect (cutting force components (Fa, Fr, and Ft)) is given as:

$$Y = \varphi(\mathrm{Vc}, f, \mathrm{ap}) \tag{1}$$

A mathematical relationship between the three independent factors can be approximated by the second-order polynomial model according to Eq. (2) as follows:

$$Y = a_0 + \sum_{i=1}^{k} b_i X_i + \sum_{i,j}^{k} b_{ij} X_i X_j + \sum_{i=1}^{k} b_{ii} X_i^2 \tag{2}$$

In addition, in order to assess the appropriateness of the proposed model, analysis of variance (ANOVA) was performed. The coefficients of determination (R^2 and R^2_{adj}) express the wellness of the fit to suggested model. These values can be determined using the following equations [23]:

$$R^2 = 1 - \frac{\mathrm{SS}_{\mathrm{residual}}}{\mathrm{SS}_{\mathrm{model}} + \mathrm{SS}_{\mathrm{residual}}} \tag{3}$$

$$R^2_{\mathrm{adj}} = 1 - \frac{\mathrm{SS}_{\mathrm{residual}}/\mathrm{DF}_{\mathrm{residual}}}{(\mathrm{SS}_{\mathrm{model}} + \mathrm{SS}_{\mathrm{residual}})/(\mathrm{DF}_{\mathrm{model}} + \mathrm{DF}_{\mathrm{residual}})} \tag{4}$$

In this equation, SS is the sum of squares and DF is the degrees of freedom. Equations (5) and (6) and an F test in

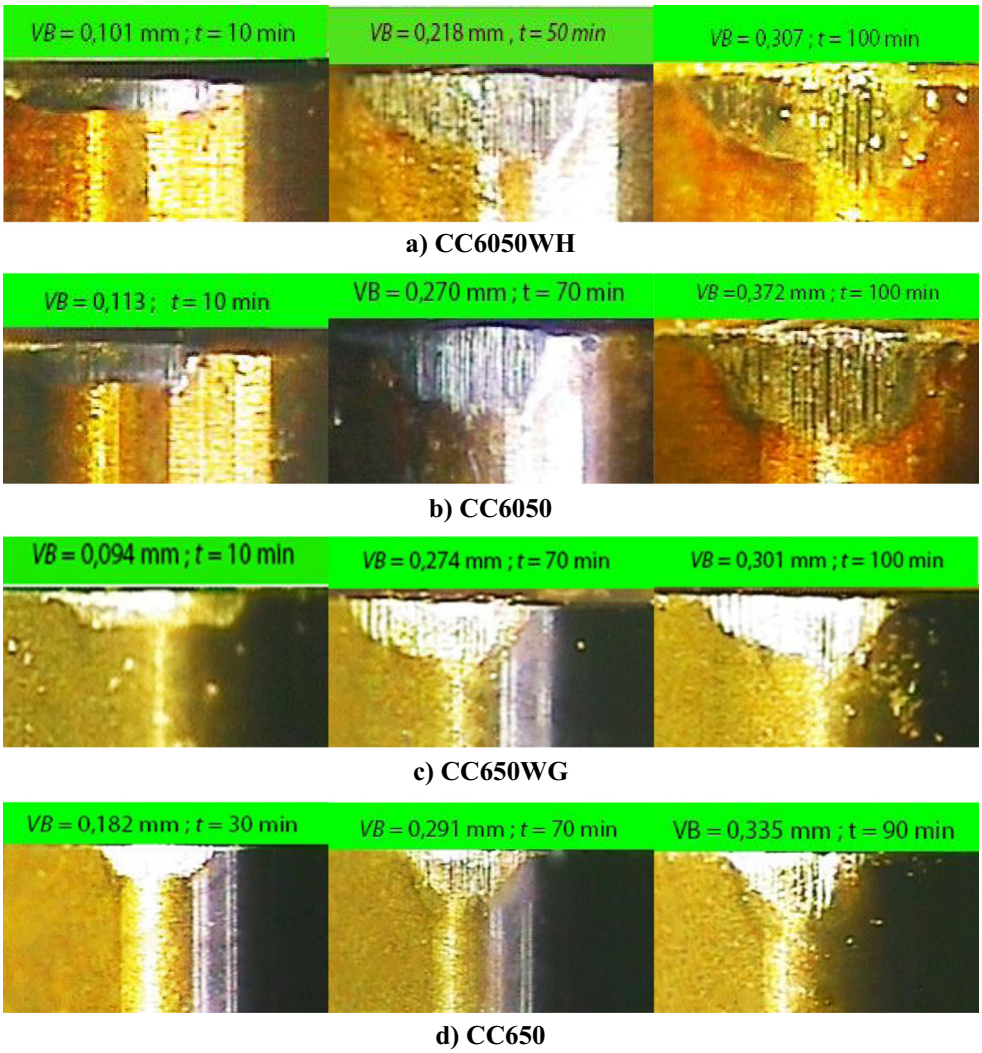

Fig. 7 Micrographs for VB of CC6050WH, CC6050, CC650WG, and CC650 at ap = 0.15 mm; f = 0.08 mm/rev, and Vc = 120 m/min. **a** CC6050WH. **b** CC6050. **c** CC650WG. **d** CC650

the program were used to check the model's adequate precision ratio (AP) to determine the statistical importance of the model :

$$\mathrm{AP} = \frac{\max(Y) - \min(Y)}{\sqrt{\overline{V}(Y)}} \tag{5}$$

$$\overline{V}(Y) = \frac{1}{n}\sum_{i=1}^{n}(Y) = \frac{p\sigma^2}{n} \tag{6}$$

Where Y is the predicted response, p represents the number of model parameters, residual mean square is described as σ^2, and n is the number of experiments. After the F test had been performed, the insignificant terms were found and eliminated from the model. Thereafter, the finalized model was introduced based on the significant variables. Eventually, optimum values were determined.

The Design-Expert software is used for the analysis of responses and determining the empirical models with best fits. Using Design-Expert, we have the facility to check the adequacy of the models using the sequential F test and the analysis of variance (ANOVA) technique.

4.1 Statistical analysis

A variance analysis of the machining forces (Fa, Fr, and Ft), was made with the objective of analyzing the influence of cutting speed, feed rate, and depth of cut on the results. In this analysis, three input parameters such as cutting speed, feed rate, and the depth of cut are being studied, and Table 1 shows the low- and high-level values of these parameters chosen. The orthogonal arrays to obtain Fa, Fr, and Ft for all cutting inserts may be observed in Table 2.

The table of ANOVA shows the degrees of freedom (DF), sum of squares (SS), mean square (MS), F values (F value), and probability (Prob.) in addition to the percentage contribution (Contr.%) of each factor and different interactions. The MS is the ratio of SS to DF, and F value is the ratio of mean

Table 1 Machining parameters

S. N °	Parameter (unit)	Level −1	Level 0	Level +1
1	Cutting speed, Vc (m/min)	80	115	150
2	Feed rate, *f* (mm/rev)	0.08	0.11	0.14
3	Depth of cut, ap (mm)	0.10	0.20	0.30

square to the mean square of the experimental error. In robust design, F value can be used for qualitative understanding of the relative factor effects. A large value of F means that the effect of a given factor is large compared to the error variance. So, the larger the value of F, the more important the given factor influencing the process response. In the same way, a low P value (Prob.) indicates statistical significance for the source on the corresponding response.

In ANOVA table, P value is the probability (ranging from 0 to 1) that the results observed in a study (or results more extreme) could have occurred by chance.

- If P value 0.05, the parameter is significant;
- If P value 0.05, the parameter is insignificant.

The other important coefficient, R^2, which is called coefficient of determination in the resulting ANOVA tables, is defined as the ratio of the explained variation to the total variation and is a measure of the fit degree. When R^2 approaches to unity, it indicates a good correlation between the experimental and the predicted values.

Tables 3, 4, 5, 6, 7, and 8 show the results of analysis of variance for cutting force components of CC6050WH, CC6050, CC650WG, and CC650 tools. This analysis was

Table 2 Experimental results for AISI 4140 machining with CC6050WH, CC6050, CC650WG, and CC650 ceramic inserts

Run N °	Machining parameters			Machining forces											
				CC6050WH			CC6050			CC650WG			CC650		
	Vc (m/min)	*f* (mm/rev)	ap (mm)	Fa (N)	Fr (N)	Ft (N)	Fa (N)	Fr (N)	Ft (N)	Fa (N)	Fr (N)	Ft (N)	Fa (N)	Fr (N)	Ft (N)
1	80	0.08	0.10	18.63	104.54	46.47	33.35	106.53	52.75	12.10	47.97	38.01	13.85	38.62	43.61
2	115	0.08	0.10	19.39	90.47	52.23	23.47	95.00	39.45	06.61	66.22	27.62	12.72	49.11	44.55
3	150	0.08	0.10	16.85	75.66	41.99	23.02	101.46	35.75	14.07	41.70	36.25	13.48	58.36	46.75
4	80	0.11	0.10	36.70	161.70	69.54	30.82	118.79	56.87	14.48	60.17	45.73	12.07	56.38	49.97
5	115	0.11	0.10	31.59	147.83	68.01	26.39	110.90	64.73	08.30	75.20	45.75	18.51	77.49	45.00
6	150	0.11	0.10	17.72	123.83	54.35	36.05	128.35	45.83	09.45	76.27	48.31	18.33	69.43	58.09
7	80	0.14	0.10	31.93	177.63	78.80	29.04	137.39	63.20	20.11	92.78	69.02	18.38	65.58	65.02
8	115	0.14	0.10	37.81	228.82	88.37	25.55	137.24	50.61	15.16	80.23	72.71	16.74	77.56	56.70
9	150	0.14	0.10	29.70	220.19	85.45	32.98	149.23	68.60	16.79	124.39	68.57	25.49	97.23	67.92
10	80	0.08	0.20	49.40	192.14	84.05	72.60	187.82	86.25	33.69	112.67	80.21	33.13	86.45	70.05
11	115	0.08	0.20	53.75	193.68	81.53	67.18	177.71	87.30	39.82	140.21	85.84	33.37	101.37	81.49
12	150	0.08	0.20	61.02	201.27	89.16	68.81	187.37	84.30	36.41	134.67	79.06	47.65	117.38	84.35
13	80	0.11	0.20	53.12	212.57	100.93	66.15	196.63	107.48	35.44	117.42	94.79	43.95	100.85	107.99
14	115	0.11	0.20	62.14	213.22	111.05	73.32	204.85	118.96	36.92	167.03	97.05	44.90	134.83	97.18
15	150	0.11	0.20	63.24	238.32	104.00	75.21	216.23	108.90	38.04	168.97	105.00	49.77	143.31	108.48
16	80	0.14	0.20	70.57	253.01	135.52	80.92	245.91	132.34	38.05	162.72	109.81	42.05	120.59	122.94
17	115	0.14	0.20	62.96	225.09	126.84	75.71	227.31	121.90	44.09	179.38	122.22	61.83	151.87	129.00
18	150	0.14	0.20	71.90	268.47	121.06	77.04	244.12	124.41	48.74	211.23	119.79	65.36	182.02	119.41
19	80	0.08	0.30	105.50	276.14	137.83	114.11	251.01	125.07	67.55	191.15	137.37	63.84	137.30	114.48
20	115	0.08	0.30	101.84	261.78	124.40	118.41	244.31	125.29	67.32	231.08	123.08	74.20	177.77	117.60
21	150	0.08	0.30	100.59	273.49	117.34	116.61	258.36	116.09	71.95	236.08	133.72	75.46	193.10	116.86
22	80	0.11	0.30	115.85	306.97	165.70	126.57	281.62	152.05	65.94	221.62	160.95	75.55	175.53	152.68
23	115	0.11	0.30	111.56	291.07	158.37	134.03	287.85	150.50	82.68	253.81	157.73	86.64	202.27	146.04
24	150	0.11	0.30	112.72	312.00	152.41	125.47	281.42	152.45	75.02	258.15	143.43	85.22	203.28	151.86
25	80	0.14	0.30	125.04	345.50	188.71	144.01	319.02	200.21	75.54	253.53	190.78	77.96	192.26	191.43
26	115	0.14	0.30	115.97	326.06	170.57	133.55	297.55	179.92	81.64	265.58	188.61	92.80	220.53	182.51
27	150	0.14	0.30	137.23	357.32	195.41	140.15	322.96	176.13	96.43	305.70	182.34	108.79	245.97	167.57

Table 3 ANOVA for axial force using TiN-coated ceramics (CC6050WH and CC6050)

Coated ceramic							
Source	DF	SS	MS	*F* value	Prob.	Cont. %	Remarks
Wiper CC6050WH							
Model		36,343.88	4038.21	107.24	0.0001		Significant
Vc	1	0.99	0.99	0.026	0.8728	0.003	Insignificant
f	1	1354.43	1354.43	35.97	0.0001	3.727	Significant
ap	1	34,320.25	34,320.25	911.41	0.0001	94.432	Significant
Vc × *f*	1	3.37	3.37	0.090	0.7684	0.009	Insignificant
Vc × ap	1	61.38	61.38	1.63	0.2189	0.169	Insignificant
f × ap	1	55.21	55.21	1.47	0.2425	0.152	Insignificant
Vc × Vc	1	10.39	10.39	0.28	0.6061	0.029	Insignificant
f × *f*	1	0.012	0.012	3.147E-4	0.9861	0.00001	Insignificant
ap × ap	1	537.83	537.83	14.28	0.0015	1.480	Significant
Résiduel	17	640.15	37.66				
Total	26	36,984.03				100	
SD = 6.14						R^2 = 0.9827	
Mean = 67.21						R^2 adjusted = 0.9735	
Coefficient of variation = 9.13						R^2 predicted = 0.9536	
Predicted residual error of sum of squares (PRESS) = 1714.22						Adequate precision = 29.525	
Conventional CC6050							
Model		45,325.3614	5036.15127	249.703996	<0.0001		Significant
Vc	1	0.27627222	0.27627222	0.01369821	0.9082	0.001	Insignificant
f	1	571.107339	571.107339	28.3168191	<0.0001	1.260	Significant
ap	1	44,227.3454	44,227.3454	2192.8938	<0.0001	97.577	Significant
Vc × *f*	1	5.09603333	5.09603333	0.25267309	0.6216	0.011	Insignificant
Vc × ap	1	0.14083333	0.14083333	0.00698284	0.9344	0.000	Insignificant
f × ap	1	308.560208	308.560208	15.2991268	0.0011	0.681	Significant
Vc × Vc	1	26.3062241	26.3062241	1.30432326	0.2693	0.058	Insignificant
f × *f*	1	2.45333519	2.45333519	0.12164202	0.7315	0.005	Insignificant
ap × ap	1	184.075741	184.075741	9.12689979	0.0077	0.406	Significant
Résiduel	17	342.864244	20.1684849				
Total	26	45,668.2257				100	
SD = 4.49						R^2 = 0.9925	
Mean = 76.69						R^2 adjusted = 0.9885	
Coefficient of variation = 5.86						R^2 predicted = 0.9801	
Predicted residual error of sum of squares (PRESS) = 908.60						Adequate precision = 41.315	

carried out for a 5 % significance level, i.e., for a 95 % confidence level. In the same manner, the value of "Prob." in Tables 3, 4, 5, 6, 7, and 8 for the model is less than 0.05 which indicates that the model is significant, which is desirable as it indicates that the terms in the model have a significant effect on the response. *F* table corresponding 95 % confidence level in calculation of process parameters accurately is $F_{1,\ 17,\ 0.05} = 4.45$.

Tables 3 and 4 show that the depth of cut has the highest statistical significance (Cont. = 94.432 %, Cont. = 97.577 %, Cont. = 94.726 %, and Cont. = 89.783 %) followed by feed rate (Cont. = 3.727 %, Cont. = 1.260 %, Cont. = 2.232 %, and Cont. = 5.097 %), whereas cutting speed (Cont. = 0.003 %, Cont. = 0.001 %, Cont. = 0.570 %, and Cont. = 3.035 %) was found to be less significant on the axial force (Fa) of CC6050WH, CC6050, CC650WG, and CC650, respectively. Similarly, from Tables 5 and 6, it can be seen that the depth of cut (Cont. = 77.271 %, Cont. = 89.09 %, Cont. = 87.547 %, and Cont. = 82.301 %) and feed rate (Cont. = 20.589 %, Cont. = 9.29 %, Cont. = 8.161 %, and Cont. = 9.531 %) have the major statistical significance as regards to radial force (Fr) of CC6050WH, CC6050, CC650WG, and CC650, respectively. This is because increased depth of cut results in increased tool work contact length [21]. Subsequently, chip thickness becomes

Table 4 ANOVA for axial force using uncoated ceramics (CC650WG and CC650)

Uncoated ceramic							
Source	DF	SS	MS	*F* value	Prob.	Cont. %	Remarks
Wiper CC650WG							
Model	9	18,854.9411	2094.99346	131.970904	<0.0001		Significant
Vc	1	107.555556	107.555556	6.77529748	0.0186	0.570	Significant
f	1	420.79005	420.79005	26.5070247	<0.0001	2.232	Significant
ap	1	17,860.5	17,860.5	1125.09484	<0.0001	94.726	Significant
Vc × *f*	1	30.624075	30.624075	1.9291167	0.1828	0.162	Insignificant
Vc × ap	1	138.380208	138.380208	8.71704927	0.0089	0.734	Significant
f × ap	1	63.066675	63.066675	3.9727886	0.0625	0.334	Insignificant
Vc × Vc	1	0.41256296	0.41256296	0.02598877	0.8738	0.002	Insignificant
f × *f*	1	53.0640907	53.0640907	3.34269112	0.0851	0.281	Insignificant
ap × ap	1	180.547919	180.547919	11.3733396	0.0036	0.958	Significant
Résiduel	17	269.869249	15.8746617				
Total	26	19,124.8104					
SD = 3.984						R^2 = 0.9859	
Mean = 42.679						R^2 adjusted = 0.9780	
Coefficient of variation = 9.335						R^2 predicted = 0.9630	
Predicted residual error of sum of squares (PRESS) = 716.623						Adequate precision = 34.088	
Conventional CC650							
Model	9	21,658.7983	2406.53315	133.981991	<0.0001		Significant
Vc	1	657.272939	657.272939	36.5931952	<0.0001	3.035	Significant
f	1	1103.87342	1103.87342	61.4573539	<0.0001	5.097	Significant
ap	1	19,445.8921	19,445.8921	1082.63597	<0.0001	89.783	Significant
Vc × *f*	1	104.902533	104.902533	5.84037263	0.0272	0.484	Significant
Vc × ap	1	127.5312	127.5312	7.10020727	0.0163	0.589	Significant
f × ap	1	178.101075	178.101075	9.91564846	0.0059	0.822	Significant
Vc × Vc	1	2.49615	2.49615	0.13897134	0.7139	0.012	Insignificant
f × *f*	1	0.7776	0.7776	0.04329232	0.8376	0.004	Insignificant
ap × ap	1	37.95135	37.95135	2.11291395	0.1643	0.175	Insignificant
Résiduel	17	305.347481	17.9616165				
Total	26	21,964.1458				100	
SD = 4.2381						R^2 = 0.9861	
Mean = 48.5667						R^2 adjusted = 0.9787	
Coefficient of variation = 8.7264						R^2 predicted = 0.9674	
Predicted residual error of sum of squares (PRESS) = 716.4332						Adequate precision = 36.379	

significant that causes the growth of the volume of deformed metal; requires greater cutting forces to cut the chip. On the other hand, as the feed rate is increased, the region of sheared chip increases, since resistance to material rupture is higher and hence requires larger efforts for chip removal [18, 19].

Finality, from Tables 7 and 8, it can be apparently seen that the depth of cut is the most important factor affecting Ft. Its contribution is Cont. = 78.707 %, Cont. = 81.478 %, Cont. = 85.597 %, and Cont. = 80.490 % for CC6050WH, CC6050, CC650WG, and CC650, respectively. The next factor influencing Ft is the depth of cut with Cont. = 19.960 %, Cont. = 13.41 %, Cont. = 13.433 %, and Cont. = 15.818 % contribution for CC6050WH, CC6050, CC650WG, and CC650, respectively. The cutting speed with (Cont. = 0.248 %, Cont. = 0.409 %, Cont. = 0.010 %, and Cont. = 0.001 % contributions, has a very weak significance effect.

4.2 Regression equations

The relationship between the factors and the performance measures were modeled by quadratic regression. The regression equations obtained were as follows.

Table 5 ANOVA for radial force using TiN-coated ceramics (CC6050WH and CC6050)

Coated ceramic							
Source	DF	SS	MS	*F* value	Prob.	Cont. %	Remarks
Wiper CC6050WH							
Model	9	1.449E+5	16,101.54	50.14	0.0001		Significant
Vc	1	90.45	90.45	0.28	0.6025	0.062	Insignificant
f	1	29,842.87	29,842.87	92.93	0.0001	20.589	Significant
ap	1	1.120E+5	1.120E+5	348.66	0.0001	77.271	Significant
Vc × *f*	1	709.02	709.02	2.21	0.1556	0.489	Insignificant
Vc × ap	1	122.82	122.82	0.38	0.5445	0.085	Insignificant
f × ap	1	1598.52	1598.52	4.98	0.0394	1.103	Significant
Vc × Vc	1	387.80	387.80	1.21	0.2871	0.268	Insignificant
f × *f*	1	58.57	58.57	0.18	0.6747	0.040	Insignificant
ap × ap	1	135.25	135.25	0.42	0.5250	0.093	Insignificant
Résiduel	17	5459.44	321.14				
Total	26	1.504E+ 5	16,101.54			100	
SD = 17.92						R^2 = 0.9637	
Mean = 225.14						R^2 adjusted = 0.9445	
Coefficient of variation = 7.96						R^2 predicted = 0.9069	
Predicted residual error of sum of squares (PRESS) = 13,994.47						Adequate precision = 23.927	
Conventional CC6050							
Model	9	1.321E+5	14,673.05	358.45	<0.0001		Significant
Vc	1	111.40	111.40	2.72	0.1174	0.085	Insignificant
f	1	12,332.87	12,332.87	301.28	<0.0001	9.29	Significant
ap	1	1.183E+5	1.183E+5	2889.84	<0.0001	89.09	Significant
Vc × *f*	1	12.32	12.32	0.30	0.5904	0.009	Insignificant
Vc × ap	1	2.29	2.29	0.056	0.8159	0.002	Insignificant
f × ap	1	351.87	351.87	8.60	0.0093	0.265	Significant
Vc × Vc	1	527.53	527.53	12.89	0.0023	0.387	Significant
f × *f*	1	25.38	25.38	0.62	0.4419	0.02	Insignificant
ap × ap	1	399.68	399.68	9.76	0.0062	0.301	Significant
Résiduel	17	695.89	40.93				
Total	26	1.328E+5	14,673.05			100	
SD = 6.40						R^2 = 0.9948	
Mean = 204.33						R^2 adjusted = 0.9920	
Coefficient of variation = 3.13						R^2 predicted = 0.9879	
Predicted residual error of sum of squares (PRESS) = 1602.39						Adequate precision = 58.280	

The empirical models developed for the axial force are given below in Eqs. (7)–(10). Its coefficient of correlation R^2 is 98.27, 99.25, 98.59, and 98.61 % for CC6050WH, CC6050, CC650WG, and CC650, respectively.

$$\begin{aligned} Fa_{CC6050WH} = {} & 29.738 - 0.245Vc + 77.236f - 95.017ap \\ & + 0.505Vc \times f + \ 0.6464Vc \times ap + 715f \\ & \times ap + 1.074 \times 10^{-3}Vc^2 + \ 49.383\,f^2 \\ & + 946.778ap^2 \end{aligned} \quad (7)$$

$$\begin{aligned} Fa_{CC6050} = {} & 33.129 - 0.459Vc - 65.361f + 91.762ap + 0.621Vc \\ & \times f - 0.031Vc \times ap + 1690.278f \times ap + 1.709 \\ & \times 10^{-3}Vc^2 - 710.494f^2 + 533.889ap^2 \end{aligned} \quad (8)$$

$$\begin{aligned} Fa_{CC650WG} = {} & 71.233 - 0.341Vc - 893.581f - 100.057ap \\ & + 1.521Vc \times f + \ 0.970Vc \times ap + 764.166f \\ & \times ap + 2.14 \times 10^{-4}Vc^2 + \ 3304.32f^2 + 548.555ap^2 \end{aligned} \quad (9)$$

Table 6 ANOVA for radial force using uncoated ceramics (CC650WG and CC650)

Uncoated ceramic							
Source	DF	SS	MS	*F* value	Prob.	Cont. %	Remarks
Wiper CC650WG							
Model	9	152,805.905	16,978.4339	133.070922	<0.0001		Significant
Vc	1	4904.79094	4904.79094	38.4420058	<0.0001	3.210	Significant
f	1	12,470.9425	12,470.9425	97.7428086	<0.0001	8.161	Significant
ap	1	133,777.23	133,777.23	1048.49831	<0.0001	87.547	Significant
Vc × *f*	1	427.571408	427.571408	3.35115253	0.0847	0.280	Insignificant
Vc × ap	1	708.249675	708.249675	5.55100889	0.0307	0.463	Significant
f × ap	1	52.041675	52.041675	0.40788413	0.5316	0.034	Insignificant
Vc × Vc	1	186.260817	186.260817	1.45984599	0.2435	0.122	Insignificant
f × *f*	1	118.54815	118.54815	0.92913821	0.3486	0.078	Insignificant
ap × ap	1	160.270017	160.270017	1.25613935	0.2780	0.105	Insignificant
Résiduel	17	2169.01913	127.589361				
Total	26	154,974.924				100	
SD = 11.295						R^2 = 0.9860	
Mean = 158.367						R^2 adjusted = 0.9786	
Coefficient of variation = 7.132						R^2 predicted = 0.9633	
Predicted residual error of sum of squares (PRESS) = 5682.9231						Adequate precision = 37.542	
Conventional CC650							
Model	9	90,557.5963	10,061.9551	180.314277	<0.0001		Significant
Vc	1	6291.42836	6291.42836	112.744923	<0.0001	6.947	Significant
f	1	8630.79014	8630.79014	154.667225	<0.0001	9.531	Significant
ap	1	74,530.1701	74,530.1701	1335.61058	<0.0001	82.301	Significant
Vc × *f*	1	135.4752	135.4752	2.42776999	0.1376	0.150	Insignificant
Vc × ap	1	441.896033	441.896033	7.91895438	0.0119	0.488	Significant
f × ap	1	264.234675	264.234675	4.73519149	0.0439	0.292	Significant
Vc × Vc	1	192.515585	192.515585	3.4499566	0.0807	0.213	Insignificant
f × *f*	1	3.46053519	3.46053519	0.06201418	0.8063	0.004	Insignificant
ap × ap	1	67.6256463	67.6256463	1.21187874	0.2863	0.075	Insignificant
Résiduel	17	948.639455	55.8023209				
Total	26	91,506.2358				100	
SD = 7.4701						R^2 = 0.9896	
Mean = 128.7570						R^2 adjusted = 0.9841	
Coefficient of variation = 5.8017						R^2 predicted = 0.9749	
Predicted residual error of sum of squares (PRESS) = 2298.5969						Adequate precision = 46.166	

$$\mathrm{Fa}_{\mathrm{CC650}} = 26.006 - 0.202\mathrm{Vc} - 407.621f - 20.289\mathrm{ap} + 2.815\mathrm{Vc} \times f + 0.931\mathrm{Vc} \times \mathrm{ap} + 1284.166f \times \mathrm{ap} - 5.265 \times 10^{-4}\mathrm{Vc}^2 + 400f^2 + 251.5\mathrm{ap}^2 \quad (10)$$

$$\mathrm{Fr}_{\mathrm{CC6050WH}} = 76.909 - 2.433\mathrm{Vc} + 521.978f + 916.868\mathrm{ap} + 7.321\mathrm{Vc} \times f + 0.914\mathrm{Vc} \times \mathrm{ap} - 3847.222f \times \mathrm{ap} + 6.563 \times 10^{-3}\mathrm{Vc}^2 + 3471.605f^2 + 474.778\mathrm{ap}^2 \quad (11)$$

The empirical models developed for the radial force are given in Eqs. (11)–(14). Its coefficient of correlation R^2 is 96.37, 99.48, 98.60, and 98.96 % for CC6050WH, CC6050, CC650WG, and CC650, respectively.

$$\mathrm{Fr}_{\mathrm{CC6050}} = 81.147 - 1.771\mathrm{Vc} - 102.206f + 952.936\mathrm{ap} + 0.965\mathrm{Vc} \times f - 0.125\mathrm{Vc} \times \mathrm{ap} - 1805f \times \mathrm{ap} + 7.654 \times 10^{-3}\mathrm{Vc}^2 + 2285.185f^2 - 816.167\mathrm{ap}^2 \quad (12)$$

Table 7 ANOVA for tangential force using TiN-coated ceramics (CC6050WH and CC6050)

Coated ceramic							
Source	DF	SS	MS	*F* value	Prob.	Cont. %	Remarks
Wiper CC6050WH							
Model		48,104.03	5344.89	95.51	0.0001		Significant
Vc	1	119.51	119.51	2.14	0.1622	0.248	Insignificant
f	1	9601.75	9601.75	171.58	0.0001	19.960	Significant
ap	1	37,861.10	37,861.10	676.57	0.0001	78.707	Significant
Vc × *f*	1	29.30	29.30	0.52	0.4792	0.061	Insignificant
Vc × ap	1	16.47	16.47	0.29	0.5945	0.034	Insignificant
f × ap	1	332.75	332.75	5.95	0.0260	0.692	Significant
Vc × Vc	1	0.66	0.66	0.012	0.9146	0.001	Insignificant
f × *f*	1	0.17	0.17	2.958E-3	0.9573	0.0001	Insignificant
ap × ap	1	142.33	142.33	2.54	0.1292	0.296	Insignificant
Résiduel	17	951.33	55.96				
Total	26	49,055.36	5344.89			100	
SD = 7.48						R^2 = 0.9806	
Mean = 109.26						R^2 adjusted = 0.9703	
Coefficient of variation = 6.85						R^2 predicted = 0.9469	
Predicted residual error of sum of squares (PRESS) = 2603.12						Adequate precision = 31.426	
Conventional CC6050							
Model		54,342.75	6038.08	117.04	<0.0001		Significant
Vc	1	225.85	225.85	4.38	0.0517	0.409	Insignificant
f	1	7404.23	7404.23	143.52	<0.0001	13.41	Significant
ap	1	44,992	44,992	872.12	<0.0001	81.478	Significant
Vc × *f*	1	0.15	0.15	2.815E-3	0.9583	9.05E-5	Insignificant
Vc × ap	1	8.37	8.37	0.16	0.6922	1.5E-4	Insignificant
f × ap	1	1526.64	1526.64	29.59	<0.0001	2.764	Significant
Vc × Vc	1	2.39	2.39	0.046	0.8321	0.004	Insignificant
f × *f*	1	39.13	39.13	0.76	0.3959	0.071	Insignificant
ap × ap	1	143.99	143.99	2.79	0.1131	0.261	Insignificant
Résiduel	17	877.02	51.59				
Total	26	55,219.76	6038.08			100	
SD = 7.18						R^2 = 0.9841	
Mean = 104.72						R^2 adjusted = 0.9757	
Coefficient of variation = 6.86						R^2 predicted = 0.9552	
Predicted residual error of sum of squares (PRESS) = 2472.89						Adequate precision = 33.776	

$$\mathrm{Fr}_{\mathrm{CC650WG}} = -9.542 + 0.453\mathrm{Vc} - 1001.765f + 326.577\mathrm{ap} + 5.685\mathrm{Vc} \times f + 2.195\mathrm{Vc} \times \mathrm{ap} + 694.167f \times \mathrm{ap} - 4.548 \times 10^{-3}\mathrm{Vc}^2 + 4938.889f^2 + 516.833\mathrm{ap}^2 \quad (13)$$

$$\mathrm{Fr}_{\mathrm{CC650}} = -82.776 + 0.899\mathrm{Vc} + 234.716f + 137.737\mathrm{ap} + 3.20\mathrm{Vc} \times f + 1.734\mathrm{Vc} \times \mathrm{ap} + 1564.167f \times \mathrm{ap} - 4.624 \times 10^{-3}\mathrm{Vc}^2 - 843.827f^2 + 335.722\mathrm{ap}^2 \quad (14)$$

The empirical models developed for the tangential force are given in Eqs. (15)–(18). Its coefficient of correlation R^2 is 98.06, 98.41, 98.98, and 99.07 % for CC6050WH, CC6050, CC650WG and CC650, respectively.

$$\mathrm{Ft}_{\mathrm{CC6050WH}} = 8.536 - 0.233\mathrm{Vc} + 288.289f + 109.222\mathrm{ap} + 1.488\mathrm{Vc} \times f - 0.335\mathrm{Vc} \times \mathrm{ap} + 1755.278f \times \mathrm{ap} + 2.712 \times 10^{-4}\mathrm{Vc}^2 - 184.568f^2 + 487.056\mathrm{ap}^2 \quad (15)$$

Table 8 ANOVA for tangential force using uncoated ceramics (CC650WG and CC650)

Uncoated ceramic							
Source	DF	SS	MS	*F* value	Prob.	Cont. %	Remarks
Wiper CC650WG							
Model	9	60,569.8907	6729.98785	183.483402	<0.0001		Significant
Vc	1	5.78	5.78	0.15758335	0.6963	0.010	Insignificant
f	1	8136.20201	8136.20201	221.821801	<0.0001	13.433	Significant
ap	1	51,846.2934	51,846.2934	1413.51433	<0.0001	85.597	Significant
Vc × *f*	1	4.876875	4.876875	0.13296096	0.7199	0.008	Insignificant
Vc × ap	1	74.9000333	74.9000333	2.04204127	0.1711	0.124	Insignificant
f × ap	1	291.461633	291.461633	7.94628062	0.0118	0.481	Significant
Vc × Vc	1	0.06826667	0.06826667	0.00186119	0.9661	0.000	Insignificant
f × *f*	1	84.4500167	84.4500167	2.30240778	0.1475	0.139	Insignificant
ap × ap	1	125.8584	125.8584	3.43134756	0.0814	0.208	Insignificant
Résiduel	17	623.543014	36.6790008				
Total	26	61,193.4337				100	
SD = 6.0563						R^2 = 0.9898	
Mean = 102.3611						R^2 adjusted = 0.9844	
Coefficient of variation = 5.9166						R^2 predicted = 0.9754	
Predicted residual error of sum of squares (PRESS) = 1502.5340						Adequate precision = 41.668	
Conventional CC650							
Model	9	51,455.1393	5717.2377	201.456419	<0.0001		Significant
Vc	1	0.5408	0.5408	0.01905599	0.8918	0.001	Insignificant
f	1	8139.17876	8139.17876	286.797557	<0.0001	15.818	Significant
ap	1	41,416.3387	41,416.3387	1459.37387	<0.0001	80.490	Significant
Vc × *f*	1	163.614675	163.614675	5.76523634	0.0281	0.318	Significant
Vc × ap	1	110.777633	110.777633	3.90343493	0.0646	0.215	Insignificant
f × ap	1	1583.32213	1583.32213	55.7909998	<0.0001	3.077	Significant
Vc × Vc	1	28.6307852	28.6307852	1.00885353	0.3293	0.056	Insignificant
f × *f*	1	2.81991852	2.81991852	0.09936454	0.7564	0.005	Insignificant
ap × ap	1	9.91591852	9.91591852	0.34940395	0.5622	0.019	Insignificant
Résiduel	17	482.451944	28.3795261				
Total	26	51,937.5913				100	
SD = 5.3272						R^2 = 0.9907	
Mean = 101.4641						R^2 adjusted = 0.9858	
Coefficient of variation = 5.2504						R^2 predicted = 0.9743	
Predicted residual error of sum of squares (PRESS) = 1332.6512						Adequate precision = 46.861	

$$\mathrm{Ft}_{\mathrm{CC6050}} = -22.021 - 0.183\mathrm{Vc} + 536.347f + 309.778\mathrm{ap} + 0.105\mathrm{Vc} \times f - 0.238\mathrm{Vc} \times \mathrm{ap} + 3759.722f \times \mathrm{ap} + 5.152 \times 10^{-4}\mathrm{Vc}^2 - 2837.654f^2 - 489.889\mathrm{ap}^2 \quad (16)$$

$$\mathrm{Ft}_{\mathrm{CC650WG}} = 10.618 + 0.0397\mathrm{Vc} - 606.765f + 254.871\mathrm{ap} + 0.607\mathrm{Vc} \times f - 0.714\mathrm{Vc} \times \mathrm{ap} + 1642.777f \times \mathrm{ap} + 8.707 \times 10^{-5}\mathrm{Vc}^2 + 4168.51f^2 + 458\mathrm{ap}^2 \quad (17)$$

$$\mathrm{Ft}_{\mathrm{CC650}} = -44.145 + 0.1552\mathrm{Vc} + 515.034f + 209.753\mathrm{ap} - 3.516\mathrm{Vc} \times f - 0.868\mathrm{Vc} \times \mathrm{ap} + 3828.889f \times \mathrm{ap} + 1.783 \times 10^{-3}\mathrm{Vc}^2 - 761.728f^2 - 128.55\mathrm{ap}^2 \quad (18)$$

To view better the results of the analysis of variance, Pareto graphs are built (Figs. 8, 9, and 10). These figures rank the cutting parameters and their interactions of their growing influence on the axial force (Fa), radial

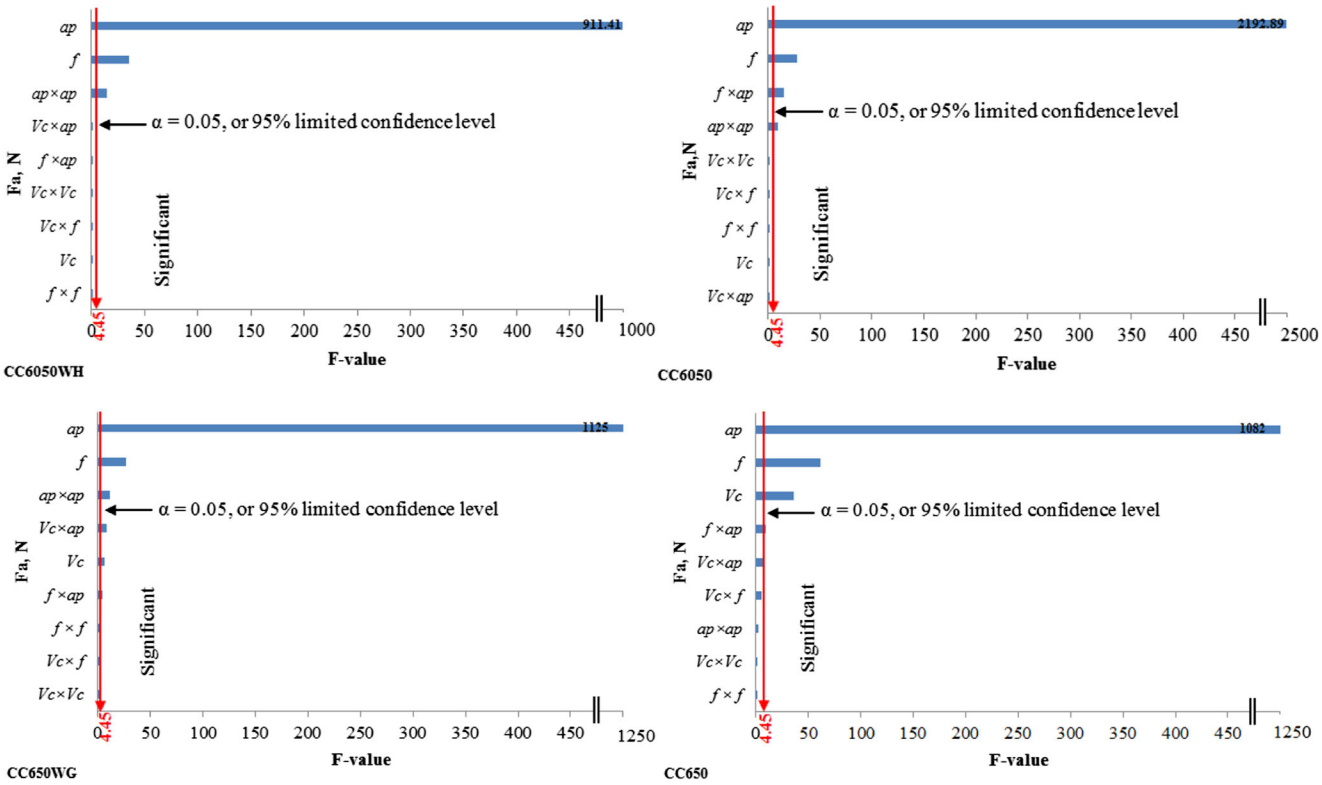

Fig. 8 Graphs of Pareto, for effect cutting parameters on axial force of CC6050WH, CC6050, CC650WG, and CC650

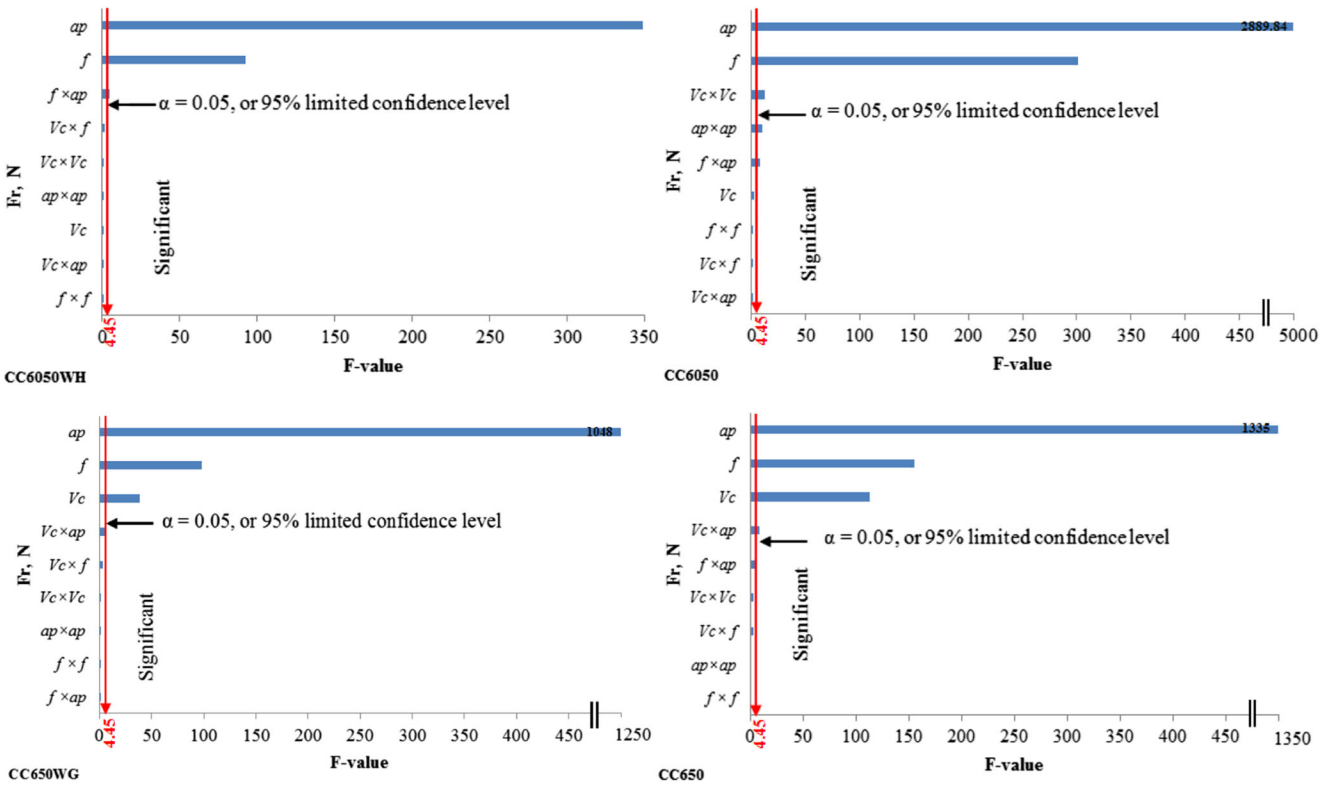

Fig. 9 Graphs of Pareto, for effect cutting parameters on radial force of CC6050WH, CC6050, CC650WG, and CC650

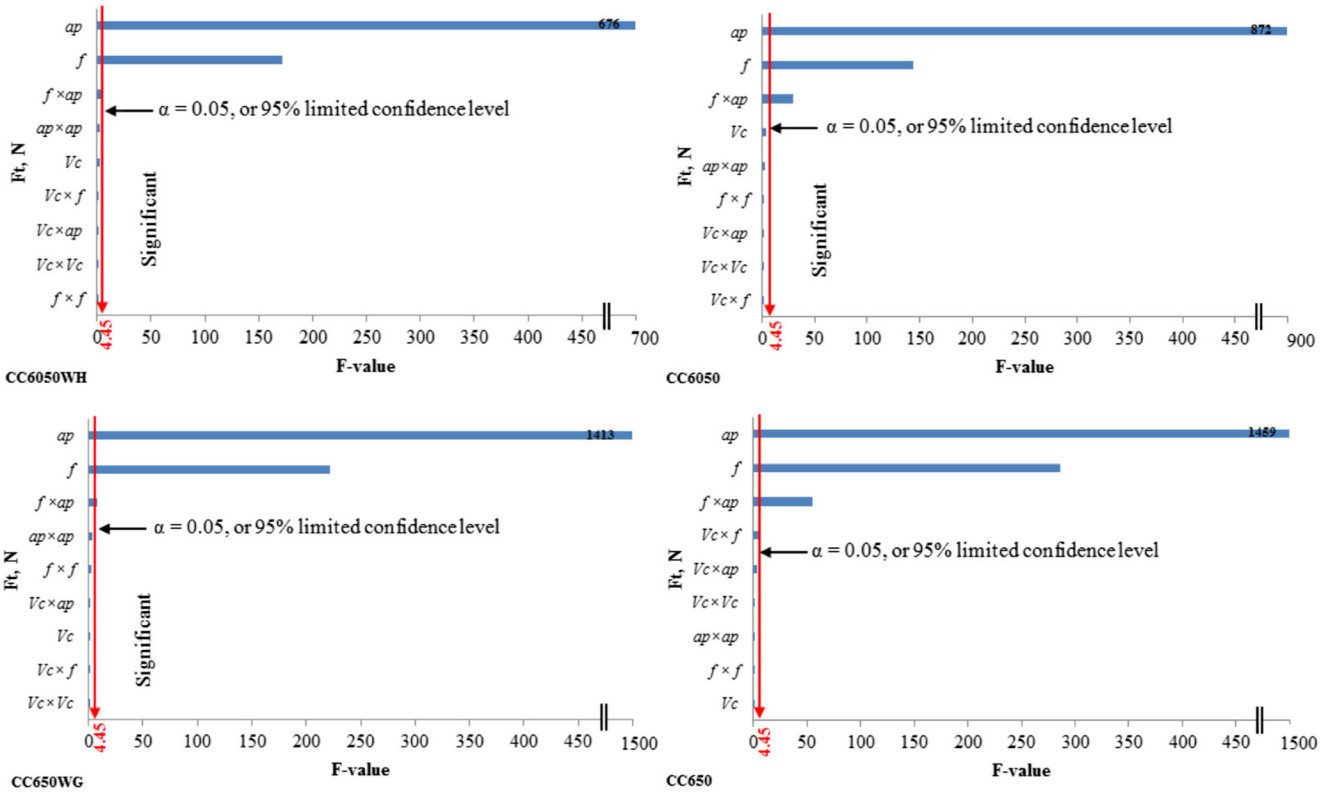

Fig. 10 Graphs of Pareto, for effect cutting parameters on tangential force of CC6050WH, CC6050, CC650WG, and CC650

force (Fr)m and tangential force (Ft). The standardized values in these figures are obtained by dividing the effect of each factor by the error on the estimated value of the corresponding factor.

The resulting Pareto graphs for the reduced quadratic model for output responses (machining forces) are shown in Figs. 8, 9, and 10. If the F table values are greater than 4.45, the effects are significant. If the values of F table are less than 4.45, the effects are not significant. In this case, the insignificant model terms can be removed. So the final Eqs. (19)–(30) of cutting force components can be written in terms of actual factor.

For axial force Fa, the regression equations formed are as follows:

$$\mathrm{Fa_{CC6050WH}} = -21.138 + 0.0067\mathrm{Vc} + 289.148f + 57.944\mathrm{ap} + 946.778\mathrm{ap}^2 R^2 = 97.92\,\% \quad (19)$$

$$\mathrm{Fa_{CC6050}} = 12.95 - 0.0035\mathrm{Vc} - 105.296f + 88.202\mathrm{ap} + 1690.278f \times \mathrm{ap} + 533.889\mathrm{ap}^2 R^2 = 99.17\,\% \quad (20)$$

$$\mathrm{Fa_{CC650WG}} = -5.48 - 0.124\mathrm{Vc} + 161.16f - 15.99\mathrm{ap} + 0.97\mathrm{Vc} \times \mathrm{ap} + 548.555\mathrm{ap}^2 R^2 = 97.82\,\% \quad (21)$$

$$\mathrm{Fa_{CC650}} = 19.556 - 0.323\mathrm{Vc} - 319.621f - 80.31\mathrm{ap} + 2.81\mathrm{Vc} \times f + 0.931\mathrm{Vc} \times \mathrm{ap} + 1284.166f \times \mathrm{ap} R^2 = 98.42\,\% \quad (22)$$

For radial force Fr, the regression equations formed are:

$$\mathrm{Fr_{CC6050WH}} = -173.909 + 0.064\mathrm{Vc} + 2126.70f + 1211.89\mathrm{ap} - 3847.221f \times \mathrm{ap} R^2 = 95.43\,\% \quad (23)$$

$$\mathrm{Fr_{CC6050}} = 45.52 - 1.689\mathrm{Vc} + 511.518f + 938.588\mathrm{ap} + 1805f \times \mathrm{ap} - 0.0076\mathrm{Vc}^2 - 816.166\mathrm{ap}^2 R^2 = 99.45\,\% \quad (24)$$

$$\mathrm{Fr_{CC650WG}} = -114.317 + 0.032\mathrm{Vc} + 877.388f + 609.669\mathrm{ap} + 2.195\mathrm{Vc} \times \mathrm{ap} R^2 = 97.99\,\% \quad (25)$$

$$\mathrm{Fr_{CC650}} = -67.36 + 0.187\mathrm{Vc} + 417.07f + 272.02\mathrm{ap} + 1.73\mathrm{Vc} \times \mathrm{ap} + 1564.167f \times \mathrm{ap} R^2 = 98.53\,\% \quad (26)$$

For tangential force *Ft*, the regression equations formed are:

$$\mathrm{Ft}_{\mathrm{CC6050WH}} = -20.006 - 0.073\mathrm{Vc} + 418.81f + 265.547\mathrm{ap} + 1755.277f \times \mathrm{ap} R^2 = 97.68\,\% \quad (27)$$

$$\mathrm{Ft}_{\mathrm{CC6050}} = 24.71 - 0.101\mathrm{Vc} - 75.88f + 8.38\mathrm{ap} + 3759.722f \times ER^2 = 98.06\,\% \quad (28)$$

$$\mathrm{Ft}_{\mathrm{CC650WG}} = -44.92 - 0.016\mathrm{Vc} + 380.129f + 355.98\mathrm{ap} + 1642.777f \times \mathrm{ap} R^2 = 98.51\,\% \quad (29)$$

$$\mathrm{Ft}_{\mathrm{CC650}} = 11.22 + 0.005\mathrm{Vc} - 56.96f + 58.5\mathrm{ap} + 3828.889f \times \mathrm{ap} R^2 = 98.46\,\% \quad (30)$$

Figure 11 shows the comparison between the predicted and measured values of machining forces (Fa, Fr, and Ft). It is concluded that the results of the comparison prove that predicted values of the cutting force component and surface roughness are very close to those experimentally recorded.

Figure 12 represents perturbation plot for the Fa, Fr, and Ft, in which the line represented by the different factors, cutting speed (Fig. 12a), feed rate (Fig. 12b), and depth of cut (Fig. 12c) revealed their individuals behaviors on Fa, Fr, and Ft, respectively, keeping other parameters constants. Figure 12 depicts an increasing trend of machining forces by increasing the feed rate (Fig. 12b) and depth of cut (Fig. 12c), whereas a decreasing trend with increase in cutting speed (Fig. 12a).

4.3 Influence of process parameters on three-component cutting forces

In order to better understand the interaction effect of variables on response factors, three-dimensional (3D) plots for the measured responses were created based on the model equations (Eqs. (7) to (18)). Since each model had three variables, one variable was held constant at the center level for each plot; therefore, a total of three response surface plots were produced for the responses (Figs. 13, 14, and 15).

Figure 13 presents the influence of cutting speed, feed rate, and depth of cut on axial force (Fa); the effects of the cutting speed, feed rate, and depth of cut on radial force (Fr) are shown in Fig. 14. Finally, the estimated surface response for tangential force, Ft in relation to the cutting speed, feed rate, and depth of cut are shown in Fig. 15.

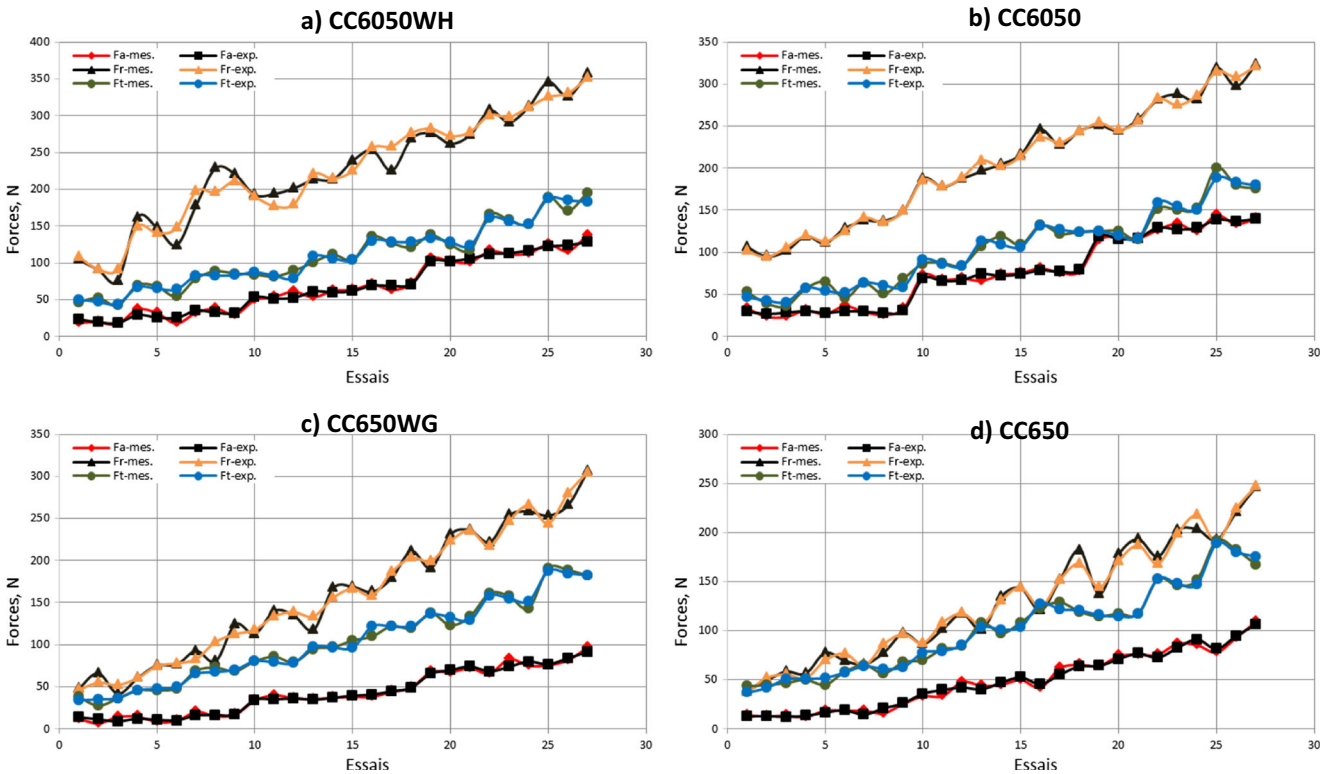

Fig. 11 Comparison between measured and predicted values for cutting force components of CC6050WH, CC6050, CC650WG, and CC650. **a** CC6050WH. **b** CC6050. **c** CC650WG. **d** CC650

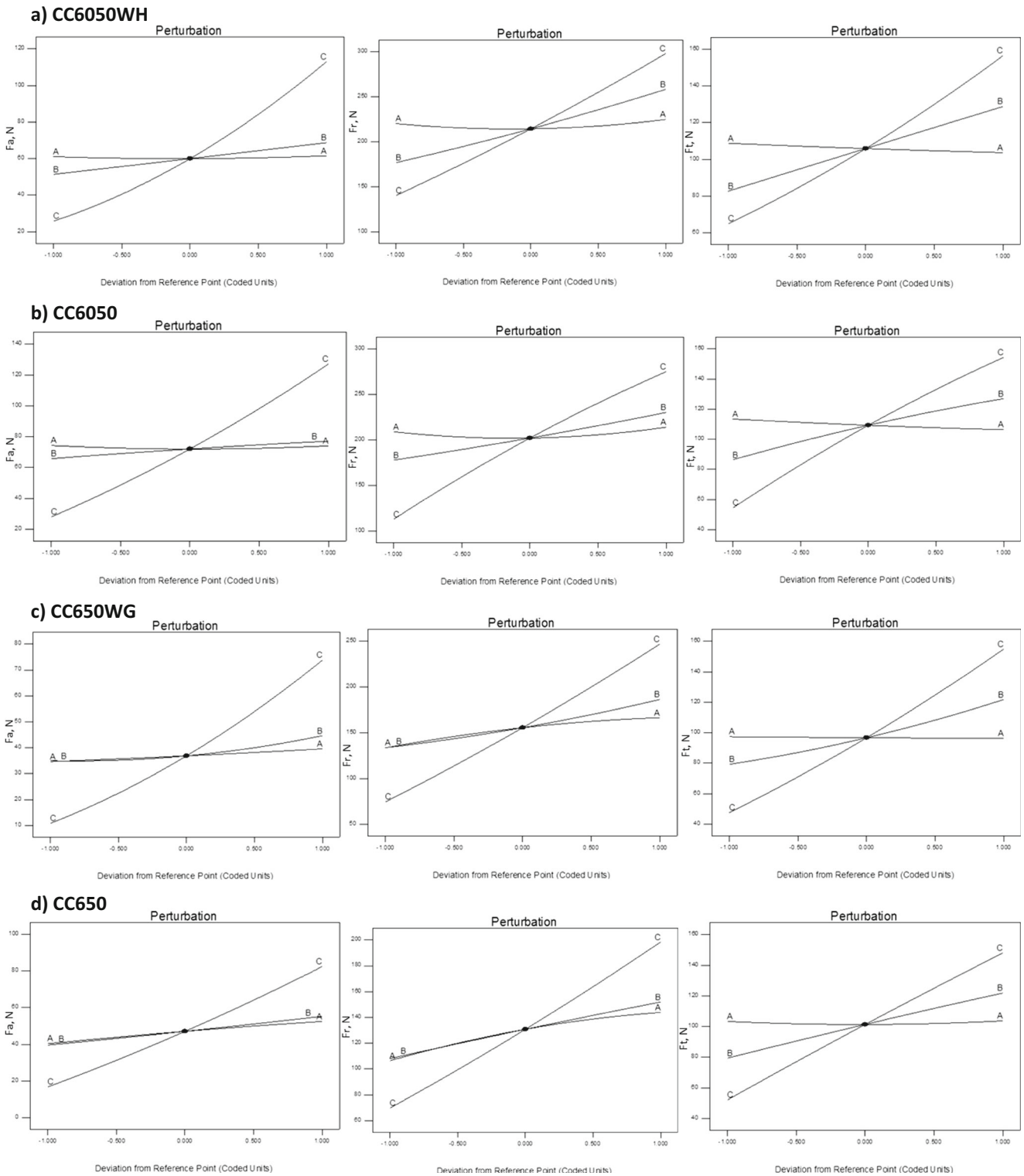

Fig. 12 Effect of machining parameters on Fa, Fr, and Ft of CC6050WH, CC6050, CC650WG, and CC650. **a** CC6050WH. **b** CC6050. **c** CC650WG. **d** CC650

The axial force increased with the increasing feed rate and depth of cut according to Fig. 13. On the other hand, the axial force decreased with the increase of the cutting speed. The lowest axial force was obtained when machining with CC6050WG tool, followed by CC650, CC6050WH, and CC6050 tools, respectively.

Figure 14 shows that the influence of the feed and depth of cut on the radial cutting force is very significant except that of

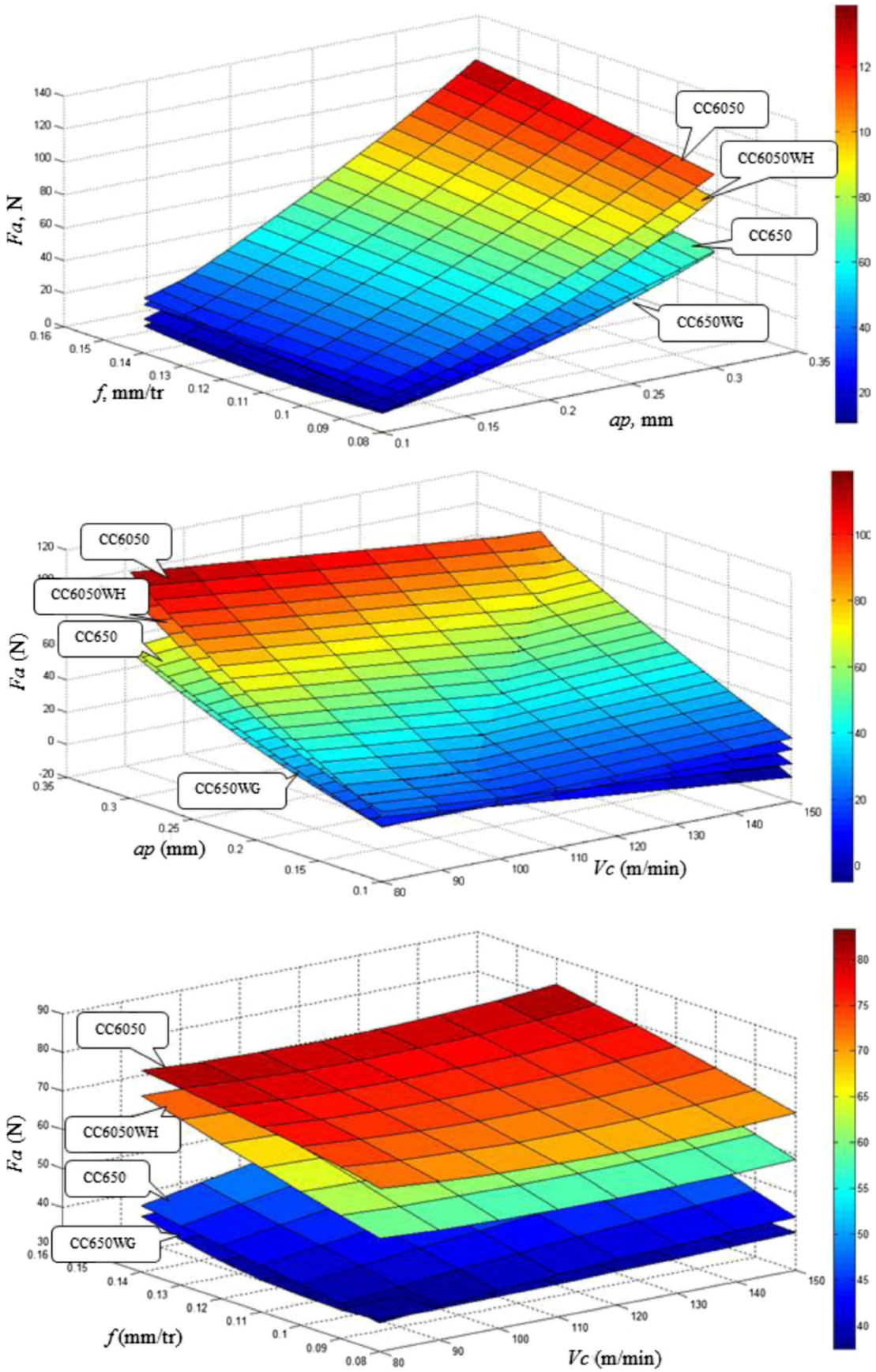

Fig. 13 3D surface plots of feed force versus Vc, *f*, and ap of CC6050WH, CC6050, CC650WG, and CC650

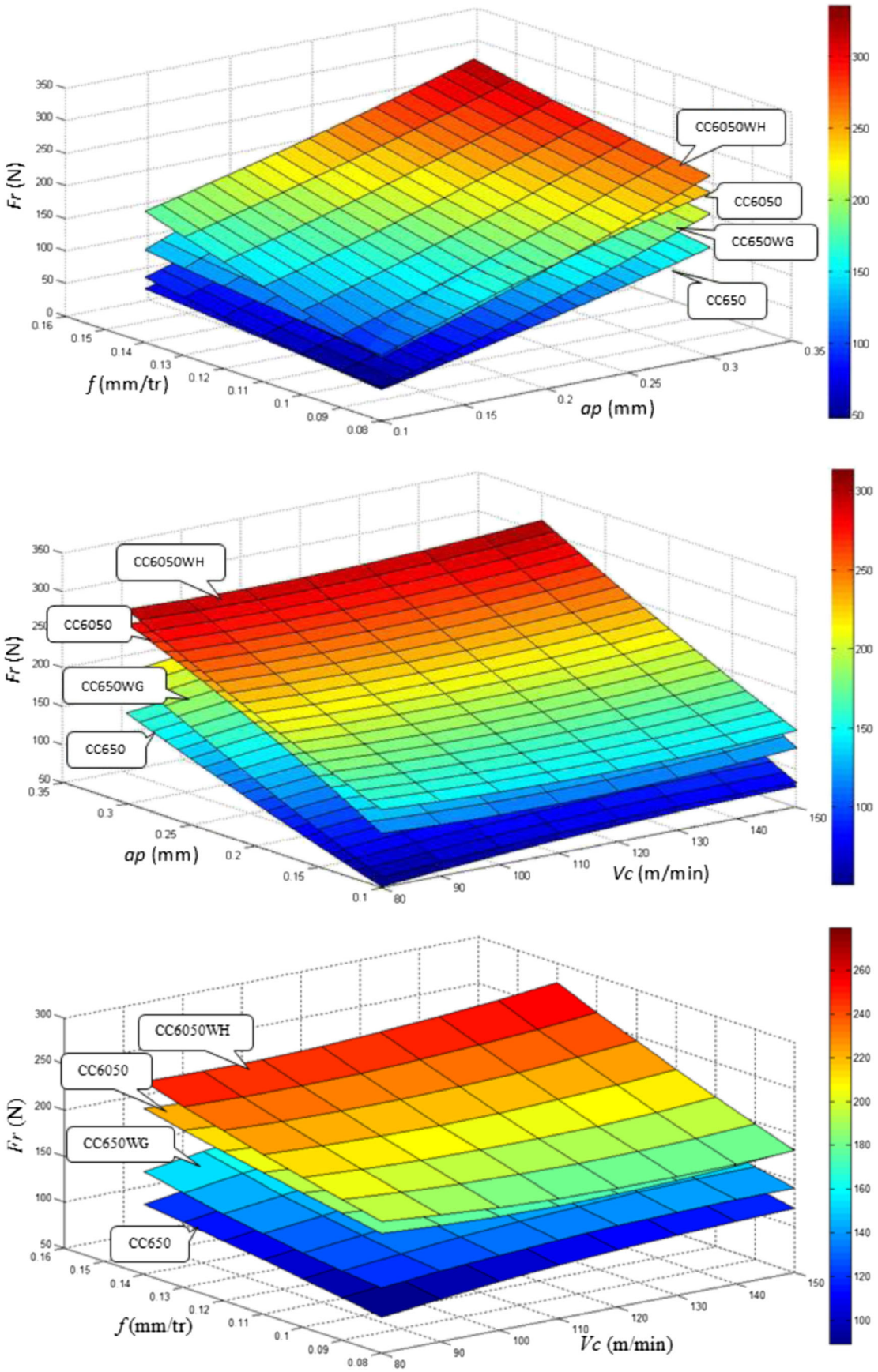

Fig. 14 3D surface plots of radial force versus Vc, *f*, and ap of CC6050WH, CC6050, CC650WG, and CC650

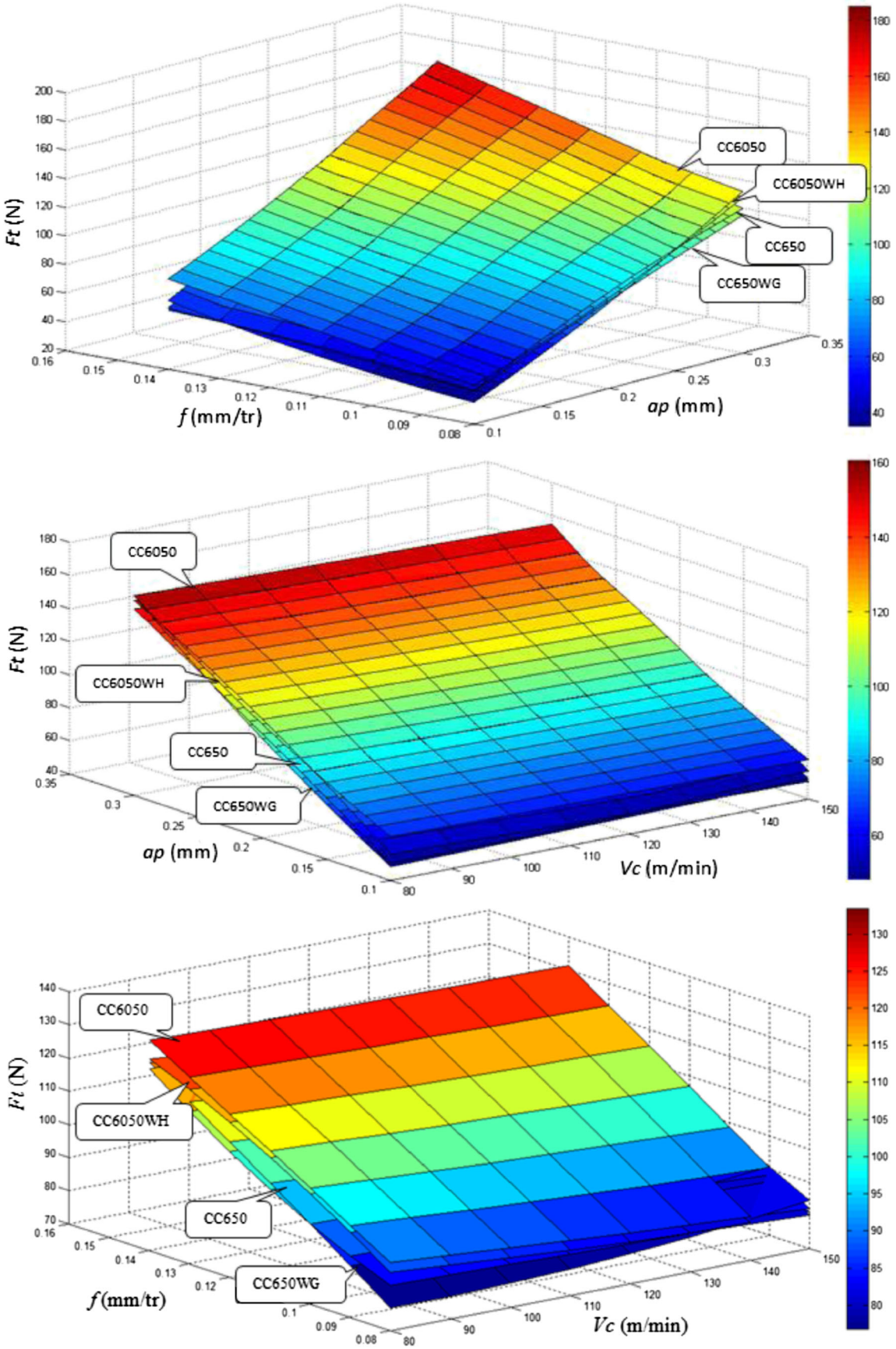

Fig. 15 3D surface plots of tangential force versus Vc, *f*, and ap of CC6050WH, CC6050, CC650WG, and CC650

Table 9 Goals and parameter ranges for optimization of cutting conditions

Conditions	Goal	Lower limit				Upper limit			
		CC6050WH	CC6050	CC650WG	CC650	CC6050WH	CC6050	CC650WG	CC650
Cutting speed, Vc (m/min)	In range	80				150			
Feed rate, *f* (mm/rev)	In range	0.08				0.14			
Depth of cut, ap (mm)	In range	0.10				0.30			
Axial force, Fa (N)	Minimize	16.85	23.02	6.61	12.07	137.23	144.01	96.43	108.79
Radial force, Fr (N)	Minimize	75.66	101.46	41.7	38.62	357.32	322.96	305.7	245.97
Tangential force, Ft (N)	Minimize	41.99	35.75	27.62	43.61	195.41	200.21	190.78	191.43

the cutting speed. It can be observed from the 3-day plots that the radial cutting force slowly increases with the increase in the cutting speed, while it nonlinearly gradually increases and then sharply increases with the increments of depth of cut. Similar results were also reported by the various researchers in literature [22, 24].

Finality, three-dimensional mapping (i.e., surface response) of Eqs. (15–18) were represented in Fig. 15a–c. As seen from Fig. 15a, b, at a constant cutting speed, tangential force increases with increases in depth of cut and feed rate. It can be seen that higher feed rate coupled with higher depth of cut significantly affects the tangential force. This can be explained as the feed rate is increased; the region of sheared chip increases, since resistance to material rupture is higher and hence requires larger efforts for chip removal [18, 19].

The analysis also shows that machining with TiN-coated ceramic inserts (CC6050WH and CC6050) generates more effort (Fa, Fr, and Ft) than the other two tested cutting ceramics (CC650WG and CC650). Besides, TiN coating made the ceramic tool gain a certain degree of toughness. This toughness caused a decrease in chipping type damage in the cutting tool. The type of wear or damage that occurs on the tool also changes the direction of chip flow. Uncoated mixed ceramic tool having lower thermal conductivity results in an increase in the temperature at the tool chip interface. This causes a thermal bimetallic effect between the upper and lower sides of the chip that forces the chip to curl a smaller radius. In addition, the radial force is found to be the larger component of turning forces.

Table 10 Response optimization for machining forces

Test N °	Machining parameters			Machining forces			Desirability	Remarks
	Vc (m/min)	*f* (mm/rev)	ap (mm)	Fa (N)	Fr (N)	Ft (N)		
CC6050WH								
1	144.70	0.08	0.10	18.0884	90	45	0.974014597	Selected
2	146.01	0.08	0.10	18.0782	90	45	0.973994138	
3	146.56	0.08	0.10	18.075	90	45	0.973974137	
CC6050								
1	122.15	0.08	0.10	26.7434	94.9993	42.2643	0.976391715	Selected
2	122.70	0.08	0.10	26.7469	95.0911	42.2246	0.976333728	
3	121.78	0.08	0.10	26.7641	95.0014	42.3235	0.97621037	
CC650WG								
1	150.00	0.08	0.10	8.99509	52.1219	36.4669	0.959848829	Selected
2	149.56	0.08	0.10	9.02078	52.2264	36.4481	0.959662119	
3	146.11	0.08	0.10	9.22342	52.9746	36.3007	0.958280354	
CC650								
1	80.00	0.08	0.10	12.6369	36.9156	36.8855	0.998042267	Selected
2	80.00	0.08	0.10	12.6453	37.2896	37.2456	0.998013372	
3	80.26	0.08	0.10	12.6501	37.2976	37.1260	0.997996648	

5 Multiple response optimizations

In this present study, desirability function optimization of the RSM has been employed for single and multiple objective optimizations [25]. During the optimization process, the main aim was to find out the optimal values of cutting parameters in order to minimize the machining forces during hard turning process. The machining forces are the main contributing factor for power requirement, motor selection, and machine tool design in machining application. These forces also affect the surface finish of the job so machinability will be good if the forces are less. The constraints used during the optimization process are summarized in Table 9. The best (optimum) cutting condition leading to the minimum machining forces are reported in Table 10 in order to decrease the desirability level. Table 10 shows the optimization results. Values of optimal cutting parameters are found to be as follows: Vc = 80 and 150 m/min, f = 0.08 mm/rev, and ap = 0.10 mm when using uncoated mixed ceramic inserts (CC650WG and CC650), respectively. The optimized machining forces are as follows: $Fa_{CC650WG}$ = 8.99 N, Fa_{CC650} = 12.63 N; $Fr_{CC650WG}$ = 52.12 N, Fr_{CC650} = 36.91 N; and $Ft_{CC650WG}$ = 36.46, Ft_{CC650} = ;36.8855 N.

6 Conclusions

In the present investigation, the various machinability aspects such as machining forces and tool wear were analyzed to study the effects of cutting speed, feed rate, depth of cut, and machining time in hard turning of AISI 4140 high-strength low alloy steel with CC6050WH, CC6050, CC650WG, and CC650 ceramic inserts. The experiments were planned as per full factorial design and the response surface methodology has been employed for the machinability study. Analysis of variance has been carried out to check the adequacy of the proposed machinability models. Based on the experimental results and the subsequent parametric analysis the following conclusions are drawn within the ranges of the process parameters selected:

- The machining forces is highly sensitive to depth of cut and feed rate in case of hard turning with TiN-coated ceramics (CC6050 and CC6050WH) as compared to uncoated mixed ceramics (CC650WG and CC650). On the other hand, cutting speed has the least effect. In general, the inserts CC650WG and CC650 provides lower values than the CC6050WH- and CC6050-coated ceramic tools.
- During machinability study in dry hard turning, it is observed that the tool life for both wiper ceramic tools (CC6050WG and CC650WH) are higher, i.e., about 19 min, 10 min for uncoated mixed ceramic (CC650) and TiN-coated ceramic tools (CC6050), respectively, under extreme cutting conditions of hard turning of AISI 4340 steel (60 HRC).
- The results of ANOVA and the validation experiments confirm that the developed mathematical model shows excellent fit and predicted values are very close to experimental values.
- The optimum values of cutting conditions are achieved with the overall desirability function. The optimum cutting conditions for machining forces are in the region of cutting speed = 80 and 150 m/min, feed rate = 0.08 mm/rev, and depth of cut = 0.10 mm when using uncoated mixed ceramic inserts (CC650WG and CC650).

ap, Depth of cut (mm); *f*, Feed rate (mm/rev); *Fa*, Axial force (N); *Fr*, Radial force (N); *Ft*, Tangential force (N); *VB*, Flank wear (mm); *V*c, Cutting speed (m/min); HRC, Rockwell hardness; α, Clearance angle (degree); γ, Rake angle (degree); λ, Inclination angle (degree); χ_r, Major cutting edge angle (degree)

References

1. Zimmermann K, Schneider GA, Bhattacharya AK, Hintze W (2007) Surface modification of Al_2O_3/TiC cutting ceramics. J Am Ceram Soc 90:3773–3778
2. Ayas E, Kara A (2004) Pressure less sintering of Al_2O_3–TiCN composites. Key Eng Mater 264–268:849–852
3. Ai X, Xiao H (1988) Ceramic cutting tool machining. China Machine Press Beijing
4. Kim S (1994) Material properties of ceramic cutting tools. Key Eng Mater 96:33–80
5. Fnides B, Aouici H, Elbah M, Boutabba S, Boulanouar L (2015) Comparison between mixed ceramic and reinforced ceramic tools in terms of cutting force components modelling and optimization when machining hardened steel AISI 4140 (60 HRC). Mech Ind 16:609
6. Aouici H, Bouchelaghem H, Yallese MA, Elbah M, Fnides B (2014) Machinability investigation in hard turning of AISI D3 cold work steel with ceramic tool using response surface methodology. Int J Adv Manuf Technol 73:1775–1788
7. Hessainia Z, Belbah A, Yallese MA, Mabrouki T, Rigal J-F (2013) On the prediction of surface roughness in the hard turning based on cutting parameters and tool vibrations. Measurement 46:1671–1681
8. Fnides B, Aouici H, Yallese MA (2008) Cutting forces and surface roughness in hard turning of hot work steel X38CrMoV5-1 using mixed ceramic. Mechanika 2(70):73–78
9. Luo SY, Liao YS, Tsai YY (1999) Wear characteristics in turning high hardened alloy steel by ceramic and CBN tools. J Mater Process Technol 88:114–121
10. Lalwani DI, Mehta NK, Jain PK (2008) Experimental investigations of cutting parameters influence on cutting forces and surface roughness in finish hard turning of MDN250 steel. J Mater Process Technol 206:167–179
11. Kumar AS, Durai AR, Sornakumar T (2006) Wear behavior of alumina based ceramic cutting tools on machining stainless steel and EN24 steel. TribolInt 39:191–197
12. Correia AE, Davim JP (2011) Surface roughness measurement in turning carbon steel AISI 1045 using wiper inserts. Measurement 44(5):1000–1005

13. Grzesik W (2008) Influence of tool wear on surface roughness in hard turning using differently shaped ceramic tools. Wear 265:327–335
14. Grzesik W, Wanat T (2006) Surface finish generated in hard turning of quenched alloy steel parts using conventional and wiper ceramic inserts. Int J Mach Tools Manuf 46:1988–1995
15. Davim JP, Figueira L (2007) Comparative evaluation of conventional and wiper ceramic tools on cutting forces, surface roughness and tool wear in hard turning AISI D2 steel. J Eng Manuf 221:625–633
16. Elbah M, Yallese MA, Aouici H, Mabrouki T, Rigal J-F (2013) Comparative assessment of wiper and conventional ceramic tools on surface roughness in hard turning AISI 4140 steel. Measurement 46(9):3041–3056
17. Bouchelaghem H, Yallese MA, Mabrouki T, Amirat A, Rigal J-F (2010) Experimental investigation and performance analyses of CBN insert in hard turning of cold work tool steel (D3). Mach Sci Technol 14:471–501
18. Yallese MA, Chaoui K, Zeghib N, Boulanouar L (2009) Hard machining of hardened bearing steel using cubic boron nitride tool. J Mater Process Technol 209:1092–1104
19. Lima JG, Avila RF, Abrao AM, Faustino M, Davim JP (2005) Hard turning AISI 4340 high strength low alloyed steel and AISI D2 cold work steel. J Mater Process Technol 169:388–395
20. Aouici H, Yallese MA, Chaoui K, Mabrouki T, Rigal J-F (2012) Analysis of surface roughness and cutting force components in hard turning with CBN tool: prediction model and cutting conditions optimization. Measurement 45:344–353
21. Gaitonde VN, Karnik SR, Figueira L, Davim JP (2009) Analysis of machinability during hard turning of cold work tool steel (Type: AISI D2). J Mater Process Technol 24(12):1373–1382
22. Senthilkumar N, Tamizharasan T, Gobikannan S (2014) Application of response surface methodology and firefly algorithm for optimizing multiple responses in turning AISI 1045 Steel. Arab J Sci Eng 39:8015–8030
23. Bouzid L, Yallese MA, Chaoui K, Mabrouki T, Boulanouar L (2014) Mathematical modeling for turning on AISI 420 stainless steel using surface response methodology. Proc I Mech E Part B: J Eng Manuf 1–17
24. Azizi MW, Belhadi S, Yallese MA, Mabrouki T, Rigal J-F (2012) Surface roughness and cutting forces modeling for optimization of machining condition in finish hard turning of AISI 52100 steel. J Mech Sci Technol 26:4105–4114
25. Meddour I, Yallese MA, Khattabi R, Elbah M, Boulanouar L (2015) Investigation and modeling of cutting forces and surface roughness when hard turning of AISI 52100 steel with mixed ceramic tool: cutting conditions optimization. Int J Adv Manuf Technol 77:1387–1399